J Math Chem (2009) 46:363–426
DOI 10.1007/s10910-008-9467-3

ORIGINAL PAPER

Multiscale modeling of polymer materials using field-theoretic methodologies: a survey about recent developments

S. A. Baeurle

Received: 25 July 2008 / Accepted: 2 September 2008 / Published online: 25 September 2008

Abstract Understanding the chemistry and physics of polymer systems challenges scientists from a wide spectrum of research areas, ranging from polymer science to molecular electronic structure theory. One of the characteristic features of polymer systems is that their physics involve a multitude of different length and time scales, which generally render the determination of their structure and physical properties on a detailed level computationally exhaustive. To overcome this difficulty, novel field-theoretic methodologies based on the mean field approximation have emerged recently and have proven to deliver useful results in the calculation of mesoscopic polymer models in the regime of high monomer concentrations. In this review we demonstrate that the field-theoretic approach is not only an useful formalism for treating highly concentrated polymer systems on the mesoscopic level of description, but that it is also a promising theoretical tool, to solve the multiscale problems arising in the calculation of physical properties of a wide variety of neutral and charged polymer materials. To this end, we show that the field-theoretic approach possesses the advantageous property to enable the treatment of all levels of description, spanning from the quantum to the continuum scale, within an unified theoretical framework. On the example of the coupling of the mesoscopic and continuum scale, we show that this specific feature constitutes a crucial advantage of field-theoretic approaches with regard to current state-of-the-art particle-based simulation methodologies for connecting different levels of description. Another major benefit relates to their favorable approximation characteristics, which permit to devise efficient approximation strategies for evaluating sophisticated polymer solution models in the low to moderate regime of monomer concentrations in a reliable way. To show this, we present novel low-cost approximation

S. A. Baeurle (✉)
Department of Chemistry & Pharmacy, Institute of Physical & Theoretical Chemistry,
University of Regensburg, 93053 Regensburg, Germany
e-mail: stephan.baeurle@chemie.uni-regensburg.de

strategies beyond the mean field level of approximation using effective renormalization concepts, originating from the domain of quantum field theory, and demonstrate their usefulness in the calculation of structure and physical properties of several polymer models, described at various levels of description.

Keywords Polymer field theories · Multiscale modeling · Beyond mean field approximations · Fluctuations

1 Introduction

Materials composed of polymers are widely found in nature and technology. Their great success is due to their remarkable variability, which permits to tailor their structure and dynamics to provide the desired physical property or functionality. Nature has made wide use of evolutionary principles through million of years, to optimize their composition and functioning in biological systems. In the last century humankind has rapidly increased their diversity and scope of application by developing new synthesis strategies and high-performance catalysts, which can produce a large variety of new exciting macromolecular architectures with unprecedented physical properties [1–4]. It has, however, quickly been acknowledged that testing all possible material configurations for all their properties, only through experimental means, can be a very time- and cost-intensive task. To alleviate the difficulty, simple empirical concepts and black-box simulation tools have been devised, to control and optimize their properties in a more directed fashion. In the last few years it has, however, increasingly been recognized that physical properties of macromolecular systems, such as e.g. thermodynamic or mechanical properties, are dramatically affected by morphologies and phenomena arising on different length and time scales [5–12]. To analyze the problem in more detail, let us first think about a single DNA molecule, whose monomeric unit is about the fraction of a nanometer, while the size of the whole chain is typically about several thousand times larger. Embedded in a cellular medium, the characteristic time scales of the macromolecule will range from femto-seconds, as in case of intra-molecular vibrations, to several seconds, which corresponds to the typical relaxation time of writhing motions of DNA in living cells [13]. Additional scales are introduced through counterions, solvent molecules as well as potential salt ions [14,15], significantly increasing the variability of DNA materials and, thus, rendering their behavior even more complex. However, multiscale problems from the biological world can even be more sophisticated, if one considers the signal transduction of photoactive proteins, where the formation or breaking of a covalent bond in a localized reaction center triggers a signal on a much larger scale in the protein environment [16,17]. Another example of similar type is the phenomenon of crack propagation in crystalline or amorphous polymer materials, which is of great importance in polymer technology. In order to enable a proper determination of the fracture energy, one requires a hierarchical and interrelated description, linking the breaking of the atomic bonds in the fracture region and the response of the surrounding medium on a micron scale [18,19]. The latter case shows quite convincingly that multiscale problems can also play a major role in high-value products, used in our daily life. A prominent

example is the mechanical relaxation of block-copolymer-based thermoplastic elastomers (TPEs), forming networks of physical crosslinks. From experimental investigations, it has recently been inferred that, in addition to their slow and ineffective stress relaxation through intrachain mechanisms, an infrequent but efficient process of chain pullout of the bridging chains is triggered at long times, in response to a nonlinear deformation [20]. As we will see in the following, this process provokes the generation of a new domain-structure at the nanoscale, determining magnitude and long-time behavior of their overall mechanical properties. From the previous examples, we clearly deduce that multiscale problems are universal and their complexity makes any attempt of understanding and controlling the chemistry and physics of polymer materials to a highly nontrivial task. Therefore, new theoretical approaches, which can explain and reliably predict their properties, are of inestimable interest and can open new perspectives for major technological innovations.

1.1 Modeling of polymer materials

A long-standing goal of physical, chemical and engineering sciences has been to develop efficient theoretical tools for understanding and predicting the physical properties of polymer materials from the knowledge of a few input parameters [21]. However, the development of such tools is particularly demanding, since generally one needs to cope with a multitude of components and interactions, which influence their structure and dynamics at the various scales. To meet this theoretical challenge, we have considered the following levels of description throughout this review:

1. quantum level ($\Delta l < 10\,\text{Å}$, $\Delta\tau < 10^{-15}\,\text{s}$);
2. atomistic level ($\Delta l = 10$–$100\,\text{Å}$, $\Delta\tau = 10^{-15}$ to $10^{-9}\,\text{s}$);
3. mesoscopic level ($\Delta l = 100$–$10000\,\text{Å}$, $\Delta\tau = 10^{-9}$ to $10^{-3}\,\text{s}$);
4. continuum level ($\Delta l > 10000\,\text{Å}$, $\Delta\tau > 10^{-3}\,\text{s}$).

The usefulness of the various levels for polymer materials is generally strongly dependent on the problem under consideration and must be judiciously selected prior to a simulation by making use of suitable analysis tools. A further indication of their usefulness can be gained by considering the characteristic relaxation time $\Delta\tau$ of a polymer material at the respective length scale Δl. A selection of typical values is given in the previous list, which can be used as a rough guideline. In the following we present the state of the art in modeling of polymer materials on each level separately, as well as simultaneously through interlinked levels.

1.1.1 Quantum level

At the *quantum level*, a polymer system is described in terms of nuclear and electronic degrees of freedom, whose behavior is determined by the many-particle wavefunction, obtained by solving the Schrödinger equation. Various ab initio quantum-chemical techniques [22] exist for solving this equation in the wavefunction representation, which are known as *wavefunction approaches*. These techniques in principle do not require empirical knowledge about the various effective interactions involved in the

system, but generally necessitate a high amount of computational power. Among the most prominent examples are the configuration interaction CI and coupled cluster CC methods, which rely on judicious perturbation expansions of the many-particle wavefunction [22]. Another particular useful approach is the density functional theory (DFT), which describes the states of the system via an energy functional depending on the density of the particles [23]. The basis of DFT is the proof of Hohenberg and Kohn [24], which states that the ground-state electronic energy is completely determined by the electron density ρ. In other words, there exists an one-to-one correspondence between the electron density of a system and the energy. The significance of this theorem is well illustrated by comparing DFT to the wavefunction approach. A wavefunction for a N-electron system contains $3N$-coordinates, three for each electron (four if the spin is included). In contrast, the electron density is the square of the wavefunction, integrated over $(N-1)$-electron coordinates, and, thus, only depends on three coordinates, independently of the number of electrons [22]. While the complexity of a wavefunction increases with the number of electrons, the electron density has the same number of variables, independently of the system size. The "only" problem is that, although it has been proven that each different density yields a different ground-state energy, the functional form connecting these two quantities is not known [22]. Therefore, the major focus of the research activities in the field of DFT is to design appropriate and transferable functionals, connecting the electron density with the energy. Unfortunately, to date even the simplest DFT scheme is computationally intractable on the quantum level for systems with more than approximately 1000 atoms, if one neglects the quantum nature of the nuclei. Since most of the physical properties of polymer materials are typically determined from systems containing more than the previously mentioned number of atoms, this restricts the usefulness of the quantum level of description for modeling polymers to carefully selected reaction centers.

1.1.2 Atomistic level

The next higher level of description, which in the following we will refer to as the *atomistic level*, can be reached by discarding the electronic degrees of freedom and replacing their interactions by effective coarse–grained interactions between the nuclei, expressed via classical potentials. In this picture the motions of the atoms are treated classically, and their trajectory is propagated deterministically or stochastically through state space, spanned by the respective particle degrees of freedom [25]. To explain this picture in more detail, let us in the following consider a system of N-particles, which is described by the following Hamiltonian [25]:

$$H(\mathbf{r},\mathbf{p}) = \sum_{i=1}^{N} \frac{\mathbf{p}_i^2}{2m_i} + \Phi(\mathbf{r}), \tag{1}$$

where the first and second term represent the kinetic and potential energy, respectively. The variables $\mathbf{r} = (\mathbf{r}_1, \ldots, \mathbf{r}_N)$ and $\mathbf{p} = (\mathbf{p}_1, \ldots, \mathbf{p}_N)$ denote the sets of atomic positions and momenta, while m_i is the mass of the ith atom. The potential energy $\Phi(\mathbf{r})$ is generally approximated by invoking the pairwise approximation [25], where

many-body effects are partially included in the effective pair potential $\Phi_{ij}^{eff}(r_{ij})$. In the absence of any external field, the potential energy can then be written as

$$\Phi(\mathbf{r}) \approx \sum_{i}^{N} \sum_{j>i}^{N} \Phi_{ij}^{eff}(r_{ij}), \tag{2}$$

where $r_{ij} = \left|\mathbf{r}_i - \mathbf{r}_j\right|$ is the distance between particle i and j. The sum over atomic pairs can comprise effective interactions between bonded and non-bonded atoms. A commonly used two-parameter potential model for describing non-bonded interactions between a pair of neutral atoms is the Lennard–Jones (LJ) 6–12 potential [25]

$$\Phi_{ij}^{eff}(r) = 4\epsilon \left[\left(\frac{\sigma}{r}\right)^{12} - \left(\frac{\sigma}{r}\right)^{6} \right], \tag{3}$$

where ϵ represents the potential well depth and σ is the pair separation at zero energy. The latter parameters are generally obtained from experiments or by performing ab initio quantum chemical calculations on small subsets of atoms. Once the force-fields are known, a broad range of *particle-based* computer simulation techniques are available to simulate the statistical behavior of the particle system under various external conditions [25–28]. For instance, a molecular dynamics (MD) simulation is conducted by numerically integrating in time t Hamilton's equations of motion,

$$\begin{aligned} \frac{d\mathbf{p}_i}{dt} &= -\frac{\partial H(\mathbf{r}, \mathbf{p})}{\partial \mathbf{r}_i}, \\ \frac{d\mathbf{r}_i}{dt} &= \frac{\partial H(\mathbf{r}, \mathbf{p})}{\partial \mathbf{p}_i}, \end{aligned} \tag{4}$$

for each of the N particles of the system [25]. In 3 dimensions, this represents a set of $6N$-first-order differential equations, which are integrated numerically by subjecting them to the initial set of particle positions and momenta as well as periodic boundary conditions, to reduce the influence of the finite size effects. The resulting trajectory must be representative and evolve a sufficiently long time in state space, to fulfill the quasi-ergodic theorem, expressed by [29]

$$\mathcal{O}_{obs} = \langle \mathcal{O} \rangle_{ens} = \lim_{t_{run} \longrightarrow \infty} \langle \mathcal{O} \rangle_{t_{run}}, \tag{5}$$

where $\mathcal{O}_{obs}$ is the macroscopic physical quantity and $\langle \mathcal{O} \rangle_{ens}$ the corresponding ensemble average, while $\langle \mathcal{O} \rangle_{t_{run}}$ is the time-average of the observable $\mathcal{O}$ over simulation time t_{run}.

Atomistic level simulations have been employed quite extensively in the past 50 years [25] and provided precious physical insights into the equilibrium properties of a multitude of physical systems, like e.g. membranes [30], proteins [30], polymers [31,32] and micellar solutions [33], etc. However, despite their great merit, they are plagued by inherent limitations within the conventional particle description, which are

worth reconsidering at this stage. First of all, there is an intrinsic time scale in Eq. 4 that depends on the form of the potential energy function. For a liquid of identical argon atoms interacting pairwise via the LJ potential, this time scale is given through $\tau = \left(m\sigma^2/\epsilon\right)^{1/2} \sim 10^{-12}$ s [34]. Considering that accurate numerical integration of Eq. 4 in the condensed liquid state typically requires a timestep Δt that is approximately two orders of magnitude smaller than τ, we get for liquid argon $\Delta t \sim 10^{-14}$ s. The simulation of such a fluid with current state-of-the-art MD techniques [26] would involve tracking the trajectories of approximately $N = 10^6$ atoms for up to 10^6 timesteps, which would represent 10 ns of real time [34]. Larger scale MD simulations can be carried out, but they generally require access to supercomputer resources that are not widely accessible [35]. With this information in mind, we can assess the computational resources that would be necessary to carry out a fully atomistic MD simulation of a poly-(styrene–butadiene–styrene) (SBS) block copolymer system of the type shown in Fig. 1. To simplify our simulation task, we restrict ourselves to a two-dimensional system and generously assign one atom per 1 Å^2 [8]. By taking into account the length scales depicted in the figures, we can easily estimate that one would need about 7×10^8 and 2×10^8 atoms, to simulate the systems on the left- and right-hand side respectively. If we now further consider that for macromolecular materials most of the interactions of atom pairs are non-bonded interactions, it can easily be demonstrated that in the limit of large molecules the computational time for calculating the force field energy grows approximately as the square of the number of atoms [22]. This quickly becomes prohibitive, if one considers the number of atoms generally involved in macromolecular simulations. Fortunately, the majority of these non-bonded contributions to the energy are very small, because the distances between most atom pairs are large. Therefore, a considerable saving in computational time can

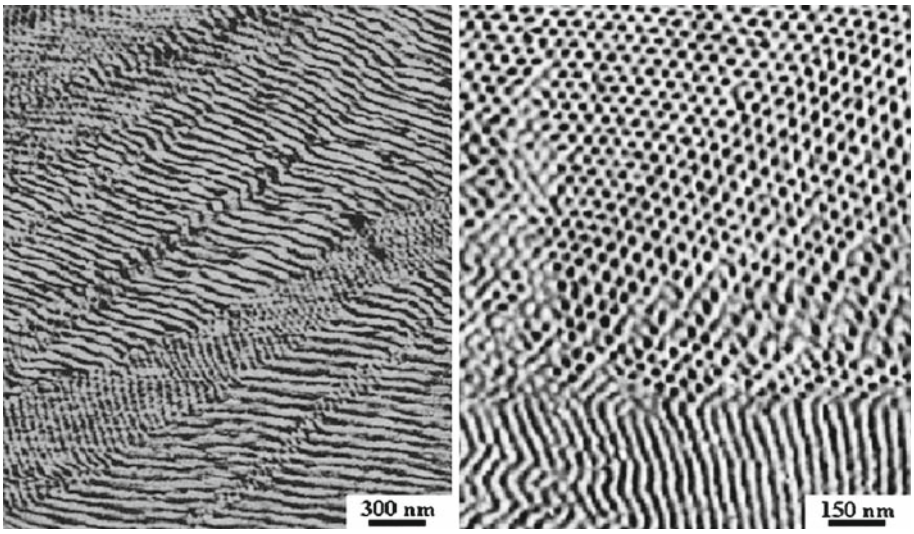

Fig. 1 Images obtained from scanning force microscopy of systems composed of phase-separated poly-(styrene–butadiene–styrene) SBS triblock copolymers [241]

be achieved by simply truncating the long-range interactions at some distance, i.e. for a system of van-der-Waals (vdW) interactions typically at 10 Å. However, it is worth taking into account that, although the contribution from most atom pairs is very small, their number becomes large very quickly and, as a consequence, they may be determinant for morphologies and phenomena on larger length scales. As a simple estimate, one can say that increasing the cutoff in a system, dominated by vdW interactions, from 10 to 20 Å increases the computational time by a factor of 5–10 [22]. In situations where such long-range interactions are important, classical DFT methodologies [23] or atomistic field-theoretic approaches of the type presented in the following [36,37] may prove more effective, because they avoid the summation over atomic pairs. Beside the length scale, another major issue to concern about in macromolecular simulations is the time scale. Adopting an argon-like timestep of 10^{-14} s for a system of macromolecular size, implies that a MD simulation with a duration of up to 10 ns would be manageable. This would certainly be enough for equilibrating a homogeneous liquid system of argon atoms. However, local equilibration of a heterogeneous block copolymer system of the size shown in Fig. 1 might take place in a time as short as 10^{-3} s, while defect migration and larger scale evolution of the composition patterns occur in seconds, hours or days [34]. The equilibration can even be longer in the vicinity of a glass transition and with longer chain lengths, since relaxation times in entangled polymer melts grow faster than the third power of the molecular weight [38]. In conclusion, we would need, at the very least, 10^5 times more computer power than is available for a current state-of-the-art MD simulation, to equilibrate the two-dimensional system considered in Fig. 1. Equilibration of a three-dimensional atomistic model of the same polymer system is to date and will remain intractable in the foreseeable future.

1.1.3 Mesoscopic level

The standard strategy for addressing the inherent difficulties, associated with fully atomistic particle-based simulations of polymer systems, is to *coarse–grain* the polymer model so that groups of atoms are lumped into larger entities, referred to as *united atoms* or *superatoms* [11,39]. The resulting effective particles may correspond e.g. to monomer residues within a polymer chain surrounded by solvent molecules, which interact by new effective interaction potentials that must be re-parameterized. Unfortunately, within the particle description it is very difficult to develop a systematic and consistent coarse–graining procedure for the large variety of polymer materials of interest. At the lowest level, one can group adjacent atoms to form an united atom (UA). For example, in case of a polyethylene polymer one can lump each CH_2-unit into an UA along the chain, and, then, use empirical knowledge or quantum chemical calculations, to fit the parameters of the respective potential models. Such an UA approach has been used quite successfully to simulate oligomeric fluids and single-phase polymeric fluids of low molecular weight, but does not go very far in alleviating the serious spatial and temporal limitations of fully atomistic simulations of polymer materials within the particle description. Higher levels of coarse–graining are even more problematic. For instance, if we wish to lump ten adjacent monomer repeat units within a polymer backbone into a single entity, the task of parameterizing the effective interactions between that entity and other such entities is very heavy. This results from

the fact that each entity consists of a subchain that can adopt many different conformations. Some success has been achieved by carrying out fully atomistic simulations of small portions of the polymer material and, then, using the simulation data to compute the spatial correlation functions among the center-of-mass positions of the subchains. These correlation functions can in principle be used to build models for effective pair, three-body, and higher inter-particle potential functions that could subsequently be employed for particle-based simulations of larger systems. In practice, however, this procedure is fraught with a number of difficulties and is far from being routine [5].

A more convenient coarse–graining procedure for a polymeric material is to essentially ignore its atomic details below a threshold of about 1 nm, while preserving larger-scale features of the individual polymers, such as their connectivity, space-filling characteristics and architecture [5,40]. The resulting techniques generally define the *mesoscopic level* of description (meso from the greek $\mu\acute{\epsilon}\sigma\eta$, which means "middle"), which designates the intermediate level between the atomistic and continuum scale. A typical example is the coarse–graining of a polypropylene–polyethylene (PP–PE) diblock copolymer into a "bead-spring" model. In such a model the positions and momenta of the atoms are centered on beads, which are interconnected by springs representing effective pair interactions between the bonded atoms along a chain. For describing the bonded interactions harmonic or anharmonic spring models are generally employed, while non-bonded interactions are treated within the pair approximation using simple empirical functions, like e.g. the LJ potential. Parameters for these potentials are typically determined by fitting simulation results to available experimental data. Such models can in general very effectively be calculated within a field-theoretic approach by making use of the mean field (MF) approximation [34]. However, a problem of this technique is that in some important cases, like e.g. neutral and charged polymer solutions in low concentrations regimes, correlations between the interacting beads are relevant and fluctuations beyond the MF level need to be taken into account, which can render the calculation very demanding. Nevertheless, it is worth noting that computer simulations of mesoscopic polymer field theories have been quite useful in studying structures and physical properties of a broad variety of important polymer systems, like e.g. polymer alloys, strongly segregated block copolymers of high molecular weight, molten polymer brushes and highly concentrated polymer solutions [34,39,41–47].

1.1.4 Continuum level

On the *continuum level* of description, one assumes the existence of a fully or partially continuous material structure in a polymer material, and in case of a composite one normally does not explicitly include the chemical interactions between the constituent phases [48]. Methods of this kind can be classified as either of analytical or numerical type. Numerical continuum-based modeling methods generally solve the continuum equations using either finite-element or finite-difference techniques. A prominent example is the finite-element (FE) method of Gusev [49,50], which uses geometries, volume fractions and other properties of the constituent phases as input for the numerical computation of the bulk properties of the composite materials. It involves the discretization of the material's representative volume element into

elements, for which the elastic solutions lead to the desired stress and strain fields [51]. In the limit of infinitely fine discretization of the FE mesh an exact numerical solution of the problem can be gained. However, it is worth mentioning that with improved discretization, the continuum-based models become more complex and corresponding FE simulations more time-consuming, which limits the utility of this approach for sophisticated polymer materials [48]. Another type of numerical continuum-based method is the boundary-element (BE) method [52], which is a continuum mechanics approach involving the solution of boundary integral equations for the evaluation of the stress and strain fields [53]. In contrast to the FE method, which necessitates elements throughout the simulation cell, this method only requires elements along the boundaries, which renders it computationally less exhaustive than the FE approach [48]. In addition, a multitude of analytical continuum-based modeling tools [48,54] have been devised in the 1960s and 1970s for solving the multiphase problems of interest, relying on a broad variety of more or less controlled model approximations. These techniques have been employed to estimate absolute values or rigorous upper/lower bounds for the mechanical properties of polymer nanocomposites [48,55–63]. A representative selection of these techniques will be discussed in more detail in Sect. 3.2.

1.1.5 Multiscale simulation

As outlined on the example of the physical problems at the beginning of this review, multiscale modeling (MSM) of polymer materials poses great challenges due to the huge range of length and time scales, influencing their structures and physical properties [9,10]. These challenges can only be met through the development of suitable hierarchical analysis and simulation strategies encompassing many interconnected levels, where each level addresses a phenomenon over a specific window of length and time. Among the various approaches, we can distinguish between two types of MSM methods, the implicit-level-coupling MSM procedures, which directly combine and simulate several levels of description within one calculation, and the hierarchical MSM procedures [6,7], in which informations from calculations at smaller scales are used as input information for calculations with coarse–grained models at larger scales. For instance, Doi and coworkers [64,65] developed a suite of hierarchical MSM tools that model polymer systems from the molecular to the continuum scale. Although each tool performs independent calculations by using only one method at a time, the output from one method can be used directly as input for another, allowing an off-line bridging between the different scales. They applied this method to study the molecular mechanism, affecting the stress–strain behavior of an ABA triblock copolymer system [31]. In their approach the problem of generating equilibrium configurations with atomistic MD is overcome by generating equilibrium configurations using information from a preliminary mesoscopic field-theoretic calculation. Kremer and coworkers developed a similar MSM strategy, to investigate the properties of polymers in contact with metal surfaces [66–68]. With this strategy, they calculated e.g. the bulk properties of a polycarbonate melt near a nickel surface by first parameterizing the surface interactions through extensive quantum-mechanical DFT calculations and, then, simulating a suitably coarse–grained bead-spring model with MD methods, using the previously determined model parameters as input parameters [66].

A multitude of additional MSM approaches have been developed in recent years aiming at bridging the atomistic–mesoscopic [39,69], atomistic–continuum [70–77], quantum–atomistic–continuum [78], as well as quantum–atomistic level of description [79,80]. However, a common feature and limitation of all these methods is the fact that portions of the system treated at different levels of resolution have to be fixed in advance and, thus, do not allow for free exchange during the simulation. This limitation is particularly problematic, if one wishes to study polymer systems, affected by severe composition fluctuations [18], like e.g. phase-separated block copolymers near the order–disorder transition or in vicinity to their interphases, polymer solutions at low to moderate monomer concentrations, etc. Note that such cases will be discussed in more detail in the subsequent parts of this review. Additional difficulties can arise by coupling methodologies of different levels of description, originating from different theoretical formalisms. In particular, translating the information between different levels, often opens severe conceptual problems, if the levels wish to be combined and simulated simultaneously. For example, atomistic particle-based methodologies are frequently connected with functional-based methodologies such as quantum DFTs, whose different theoretical framework renders a consistent treatment of the coupling region difficult. To overcome such problems, an unified theoretical framework would be highly desirable. We will demonstrate in the further development that the field-theoretic formalism is a particularly convenient language for applications involving polymers or complex fluids, since it permits to develop consistent MSM approaches from the quantum to the continuum scale within the same theoretical framework. A further substantial advantage of field-theoretic approaches with regard to particle-based methods is their high computational efficiency in dealing with macromolecular systems on the chain-level of description by making use of effective approximation strategies and their ability to treat fluctuations in an efficient way. A more detailed discussion of these issues will be given in the further development.

1.2 Main objectives and overall strategy

The main objective of this review is to provide a survey about recent progresses in the emerging field of MSM methods based on the field-theoretic formalism, and show their suitability in solving sophisticated multiple length and time scale problems arising in the determination of the physical properties of neutral and charged polymer materials. In the following we present MSM methods, which address the multiscale challenges by adopting the following two-step procedure:

1. development and application of analytical MSM and hierarchical-analysis tools, to identify the relevant length and time scales involved in the polymer system under consideration;
2. development and application of numerical MSM strategies, to study the polymer system and determine its corresponding physical properties.

In the further development we will demonstrate the effectiveness of this procedure on the example of block-copolymer-based TPEs. To this end, we make use in a preliminary step of a numerical FE tool on the continuum level of description, to study the influence of molecular details on their linear mechanical properties. Then, in a subsequent

step we introduce an analytical and numerical MSM approach, to explain and predict their peculiar long-time stress relaxation behavior, in response to a tensile deformation pertaining to the nonlinear regime of mechanical properties. The analytical MSM approach employs a semi-phenomenological ansatz, which permits to take into account within the same model the intra-chain relaxation of the dangling chains and loops, attached to the crosslinks of the polymer network, as well as the relaxation of the crosslink domains of nanoscale size, resulting from chain readjustments. This permits us to investigate the importance of the various relaxation mechanisms and to identify the relevant length and time scales, involved in the stress relaxation process at long times. We then use this information as input for developing our numerical MSM approach, which enables us to perform a more detailed investigation of the local and macroscopic physical properties of the TPEs. The numerical MSM approach introduces the continuum scale by coupling a mesoscopic field-theoretic approach with a kinetic Monte Carlo algorithm and permits in this way to simulate the fluctuations, originating from chain-dynamical processes at the interphases. To investigate the usefulness of both MSM approaches, we compare their results with mechanical experiments performed on styrenic triblock TPEs and show that they correctly describe their peculiar stress relaxation spectrum and viscoelastic behavior, observed below the glass transition temperature of the polystyrene crosslinks. A further objective of this review is to provide an overview about the recent progress made in the development of field-theoretic methodologies beyond the MF level of approximation, allowing to extend their scope of application to polymer problems, in which fluctuations are important. To this end, we present efficient low-cost approximation strategies, where fluctuation contributions are taken into account, by making use of effective quantum-field-theoretic concepts, and demonstrate their effectiveness in the calculation of structural and thermodynamic properties of polymer solutions in various concentration regimes and various levels of coarse–graining. Finally, we discuss the extension of these methodologies to real-time and quantum-statistical many-body problems, which permits us to show that the field-theoretic approach is a suitable formalism to treat all levels of description of polymer materials within an unified theoretical framework.

Our review is organized as follows. In Chapter 2 we present the basic derivation steps of the statistical field theories on the example of a system of flexible polymer chains. Afterwards, in Chapter 3 we discuss investigations of the linear mechanical behavior of styrenic triblock TPEs using the FE route and, then, present in the subsequent part our analytical and numerical MSM tools, which are employed to study the nonlinear regime. In Chapter 4 we address the fluctuation problem by introducing novel low-cost approximation strategies beyond the MF level of approximation, to treat polymer solutions in various concentration regimes on the mesoscopic level of description. Subsequently, in Chapter 5 we discuss the extension of these strategies to real-time and quantum-statistical theories. Finally, we end the review by providing conclusions and a brief outlook about future goals.

At this stage, we feel that it is important to specify that this review does not intend to give a complete overview about field-theoretic methodologies, but rather to provide a survey about recent progresses in this research area and demonstrate its potentials for MSM.

2 Statistical field theories

2.1 Basic ideas

A system with many-body interactions is generally very difficult to solve exactly within the particle-based formalism, excepting for very simple cases, like e.g. the 1D-Ising model. The great difficulty, when computing its partition-function integral and related ensemble averages, is the treatment of the many-body interaction term in the action, when integrating over all configurations. To reduce the computational burden, two major functional-based formalism have emerged in the last few years, which permit to treat multiple levels of description within an unified theoretical framework, i.e. the finite-temperature density-functional theory (FT-DFT) [81] and the statistical field-theory (SFT) [34]. The FT-DFT is applicable to both quantum and classical systems and essentially provides a formalism, how to project the multi-dimensional many-particle problem of a statistical ensemble onto a collective-variable formalism with the density field as the order parameter [23]. However, even if the Hohenberg and Kohn theorem [24] proves that a FT-DFT is an exact formalism, it does not provide any prescription, how to construct the corresponding free energy functional rendering a systematic improvement of FT-DFTs difficult in practice [22]. In contrast, the underlying concept of a SFT is to solve the combinatorial problem by exactly reformulating the partition-function integral in a suitable functional-integral representation through linearizing the action with respect to the density field $\rho(\mathbf{r})$. This is achieved by performing a delta-functional [82] or Hubbard–Stratonovich transformation [36], which permits to replace the original particle degrees of freedom with field degrees of freedom. The resulting field function $w(\mathbf{r})$ designates a set of scalar numbers defined at any position $\mathbf{r}$ in direct space, where each tuple represents a configuration pertaining to the field configuration space. To explain the field-theoretic formalism in more detail, let us in the following consider the basic derivation steps of a SFT on the example of a system of flexible polymer chains, described on the mesoscopic level of description [82].

2.2 Field theory for flexible polymer chains

The standard continuum model of flexible polymers, introduced by Edwards [83], treats a solution composed of n linear monodisperse homopolymers as a system of coarse–grained polymers, in which the statistical mechanics of the chains is described by the continuous Gaussian-thread model [34] and the solvent is taken into account implicitly. The latter model can be considered as the continuum limit of the discrete Gaussian-chain model, in which the polymers are described as beads coupled through harmonic springs. The canonical partition function of such a system, kept at an inverse temperature $\beta = 1/(k_B T)$ and confined in a volume V, can be expressed as

$$Z(n, V, \beta) = \frac{1}{n!(\lambda_T^3)^{nN}} \prod_{j=1}^{n} \int \mathcal{D}\mathbf{r}_j \exp\left(-\beta\Phi_0[\mathbf{r}] - \beta\bar{\Phi}[\mathbf{r}]\right), \tag{6}$$

where $\bar{\Phi}[\mathbf{r}]$ is the potential of mean force given by,

$$\bar{\Phi}\left[\mathbf{r}\right] \approx \frac{N^2}{2}\sum_{j=1}^{n}\sum_{k=1}^{n}\int_0^1 ds\int_0^1 ds'\bar{\Phi}\left(\left|\mathbf{r}_j(s)-\mathbf{r}_k(s')\right|\right)-\frac{1}{2}nN\bar{\Phi}(0), \tag{7}$$

representing the solvent-mediated non-bonded interactions among the segments, while $\Phi_0[\mathbf{r}]$ represents the harmonic stretching energy of the bead-spring chains. The latter energy contribution can be formulated as

$$\Phi_0[\mathbf{r}] = \frac{3k_BT}{2Nb^2}\sum_{l=1}^{n}\int_0^1 ds\left|\frac{d\mathbf{r}_l(s)}{ds}\right|^2, \tag{8}$$

where b is the statistical segment length and N the polymerization index. Moreover, we point out that the latter term in Eq. 7 denotes the self-interaction contribution of the non-bonded inter-monomer interactions. To derive the basic field-theoretic representation of the canonical partition function, we next introduce the segment density operator of the polymer system

$$\hat{\rho}(\mathbf{r}) = N\sum_{j=1}^{n}\int_0^1 ds\delta\left(\mathbf{r}-\mathbf{r}_j(s)\right). \tag{9}$$

Using this definition, we can easily rewrite Eq. 7 as

$$\bar{\Phi}\left[\mathbf{r}\right] = \frac{1}{2}\int d\mathbf{r}\int d\mathbf{r}'\hat{\rho}(\mathbf{r})\bar{\Phi}(\left|\mathbf{r}-\mathbf{r}'\right|)\hat{\rho}(\mathbf{r}')-\frac{1}{2}nN\bar{\Phi}(0). \tag{10}$$

Next, we transform the model into a SFT by making use of the definition of the delta-functional

$$\int \mathcal{D}\rho\,\delta\left[\rho-\hat{\rho}\right]F\left[\rho\right] = F\left[\hat{\rho}\right], \tag{11}$$

where $F\left[\hat{\rho}\right]$ is a functional and $\delta\left[\rho-\hat{\rho}\right]$ is the delta functional given by

$$\delta\left[\rho-\hat{\rho}\right] = \int \mathcal{D}w\, e^{i\int d\mathbf{r}w(\mathbf{r})[\rho(\mathbf{r})-\hat{\rho}(\mathbf{r})]}, \tag{12}$$

with $w(\mathbf{r}) = \sum_{\mathbf{G}} w(\mathbf{G})\exp\left[i\mathbf{G}\mathbf{r}\right]$ representing the field function. We note that, expanding the field function in a Fourier series, implies that periodic boundary conditions are applied in all directions and that the $\mathbf{G}$-vectors designate the reciprocal lattice vectors of the supercell. Making use of Eqs. 10–12, we can recast the canonical partition function in Eq. 6 into the following field-theoretic representation:

$$Z(n,V,\beta) = Z_0\int \mathcal{D}w\exp\left[-\frac{1}{2\beta V^2}\int d\mathbf{r}d\mathbf{r}'w(\mathbf{r})\bar{\Phi}^{-1}(\mathbf{r}-\mathbf{r}')w(\mathbf{r}')\right]Q^n[iw], \tag{13}$$

where

$$Z_0 = \frac{1}{n!}\left(\frac{\exp\left(\beta/2N\bar{\Phi}(0)\right)Z'}{\lambda_T^{3N}}\right)^n \tag{14}$$

can be interpreted as the partition function for an ideal gas of non-interacting polymers and

$$Z' = \int \mathcal{D}\mathbf{R}\exp\left[-\beta U_0(\mathbf{R})\right] \tag{15}$$

is the path integral of a free polymer in a zero field with elastic energy

$$U_0[\mathbf{R}] = \frac{k_B T}{4R_{g0}^2}\int_0^1 ds\left|\frac{d\mathbf{R}(s)}{ds}\right|^2. \tag{16}$$

In the latter equation the unperturbed radius of gyration of a chain $R_{g0} = \sqrt{Nb^2/(2d)}$, where the space dimension $d = 3$. Moreover, in Eq. 13 the partition function of a single polymer, subjected to the field $w(\mathbf{R})$, is given by

$$Q[iw] = \frac{\int \mathcal{D}\mathbf{R}\exp\left[-\beta U_0[\mathbf{R}] - iN\int_0^1 ds\; w(\mathbf{R}(s))\right]}{\int \mathcal{D}\mathbf{R}\exp\left[-\beta U_0[\mathbf{R}]\right]}, \tag{17}$$

with U_0 defined by Eq. 16. To derive the grand canonical partition function, we use its standard thermodynamic relation to the canonical partition function [25],

$$\Xi(\mu, V, \beta) = \sum_{n=0}^{\infty} e^{\beta\mu n} Z(n, V, \beta), \tag{18}$$

where μ is the chemical potential and $Z(n, V, \beta)$ is given by Eq. 13. After performing the sum, Eq. 18 provides the field-theoretic representation of the grand canonical partition function,

$$\Xi(\xi, V, \beta) = \gamma_{\bar{\Phi}}\int \mathcal{D}w\exp\left[-S[w]\right], \tag{19}$$

where

$$S[w] = \frac{1}{2\beta V^2}\int d\mathbf{r}d\mathbf{r}' w(\mathbf{r})\bar{\Phi}^{-1}(\mathbf{r}-\mathbf{r}')w(\mathbf{r}') - \xi Q[iw] \tag{20}$$

is the grand canonical action with $Q[iw]$ defined by Eq. 17 and the constant

$$\gamma_{\bar{\Phi}} = \frac{1}{\sqrt{2}}\prod_{\mathbf{G}}\left(\frac{1}{\pi\beta\bar{\Phi}(\mathbf{G})}\right)^{1/2}. \tag{21}$$

Moreover, the parameter related to the chemical potential

$$\xi = \frac{\exp\left(\beta\mu + \beta/2N\bar{\Phi}(0)\right) Z'}{\lambda_T^{3N}}, \tag{22}$$

where Z' is provided by Eq. 15. Similar SFTs can be derived for systems described on the quantum [84–87], atomistic [36,37] and continuum level of description [88] by performing analogous transformations. This characteristic confers SFT methods very advantageous properties over particle-based approaches for solving multiscale problems, since they permit to treat all scales within an unified theoretical framework. Another advantage of SFT approaches lies in the development of effective low-cost approximation strategies, which provide them *collective variable* character similar to FT-DFTs and the possibility of handling a fewer number of degrees of freedom. Moreover, the accuracy of SFT approximations, in contrast to FT-DFTs, can generally further be improved in a systematic way by computing higher-order corrections. As a very convincing example, we should here focus on the single field degree of freedom, obtained by invoking the MF approximation. With the sole MF configuration, one can reliably describe the state of a broad class of polymer melts and polymer solutions at high monomer concentrations, involving a large number of particle degrees of freedom and interactions. If we would instead compute such systems with conventional particle-based simulation approaches, this would certainly involve a much higher number of degrees of freedom and, as a consequence, be computationally much more demanding. A further significant advantage with respect to particle-based approaches arises in the computation of macromolecular systems with soft, long-ranged interactions [89]. As already outlined in Sect. 1.1.2 of the introduction, particle-based approaches require large cutoffs or computationally expensive techniques like the Ewald summation [25], to treat systems with long-range interactions reliably. Such techniques are not needed in case of SFT methods. Moreover, the often highly polymeric nature of macromolecular systems introduces additional difficulties for particle-based approaches, since it leads to very long equilibration times [34]. SFT methods overcome the problem by reformulating the particle systems in functional integral formulation and discarding configurations of low statistical weight through making use of effective calculation strategies. Finally, additional benefits for the latter methods are expected in the computation of open polymer systems at lower temperatures in the range of physical interest. In such situations particle-based grand canonical simulation algorithms are known to become increasingly inefficient with growing interaction strength between the interacting monomers, due to a highly ineffective particle insertion step [37,90]. Since grand canonical SFT approaches do not perform particle insertion moves, this represents another major advantage on the route towards understanding and predicting the structure–property relationship of macromolecular systems.

2.3 Mean-field approximation and fluctuation problem

A simple approximation strategy, commonly used to calculate SFTs on all levels of description, relies on the mean-field MF approximation,

$$\left.\frac{\delta S[w]}{\delta w(\mathbf{r})}\right|_{w=w_{MF}} = 0. \tag{23}$$

It reduces the computational task by replacing the many-body interaction term in the action by a term where all bodies of the system interact with an average effective field. This allows us to reduce any multi-body problem into an effective one-body problem and implies that the partition-function integral of the model under consideration is dominated by a single field configuration. A major benefit of solving problems within the MF approximation is that it provides some useful insights into the structure and physical properties of the system at relatively low computational cost and in many instances also represents a convenient launch-point, to study higher-order fluctuation corrections. Successful applications can be found throughout all fields of physics, chemistry and biology [91–95]. The MF approximation has also widely been employed to approximate functional integrals arising in SFTs of polymers and complex fluids [34,41–43]. Originally introduced in this area by Edwards [83], Helfand and Tagami [96] and commonly referred to as self-consistent field theory (SCFT), it has been proven useful for estimating structure and thermodynamic properties of a large variety of polymer systems, including polymer alloys, strongly segregated block copolymers of high molecular weight, molten polymer brushes and highly concentrated polymer solutions, among others [34]. There are, however, a multitude of important cases in polymer science, in which the MF approximation provides inaccurate or even qualitatively incorrect results [34]. These comprise neutral polymer or polyelectrolyte solutions in dilute and semidilute concentration regimes, block copolymers near their order–disorder transition, polymer blends near their phase transitions, etc. In such situations the partition-function integral, defining the field-theoretic model, is not entirely dominated by the MF configuration, and field configurations far from it can make important contributions, which require the use of more sophisticated calculation techniques beyond the MF level of approximation. In the following we will show that, in case of neutral and charged polymer solutions, the MF approximation technique gives reliable information about the system in the regime of high monomer concentrations, where the interactions among the monomers are highly screened and fluctuations away from the MF configuration are unimportant. However, it is worth considering in this context that in most biological and technological applications of polymer solutions the ranges of physical interest lie in the intermediate to low concentration regimes, where fluctuations beyond the MF level of approximation become relevant and dominate the overall physical behavior. To cope with these difficulties, we will present in Sect. 4.2.1 novel low-cost approximation techniques, which permit to take into account such fluctuation contributions effectively and in this way extend the scope of application of SFTs to lower concentration regimes.

3 Block copolymers

Block copolymers are polymers made of two or more chemically distinct sequences (blocks) of monomer units that are covalently linked together. A particular important type of block copolymers are those contained in thermoplastics [97], which are

constituted of chains with alternating hard and soft segments. Prominent examples among them are the technologically important styrenic thermoplastic elastomers TPEs. They are typically composed of triblock copolymer chains, where a center-block of either poly-isoprene (PI) or poly-butadiene (PB) is chemically connected with end-blocks of poly-styrene (PS). For high molecular weights and below the order–disorder transition temperature, such block copolymers phase-separate by forming periodically arranged networks of PS phases, embedded in a matrix phase of either PI or PB. Depending on the volume fraction of the components, the PS phases may adopt a spherical, cylindrical, gyroid or lamellar morphology, which are of nanoscale size [98]. Below the glass transition temperature of PS, the PS phases form hard glassy crosslinks, conferring these solid materials their exceptional strength and elasticity. However, as we will see in the following already at room temperature the physical crosslinks of PS can become transient in nature, which may induce viscoelastic behavior. Block copolymer-based TPEs are particularly relevant in pressure sensitive applications, where high elasticity and durability is important, like e.g. tire treads or packaging [99]. Moreover, they also show promising field of applications in nanotechnology as nanostructured self-assembling matrix-templates [100–103], providing new perspectives for large-scale industrial manufacturing of flexible color displays [104] or solar cells [105,106] at affordable production costs. Last but not least, block copolymers in solution also find wide use in medicinal applications, like e.g. amphiphilic block copolymers for drug delivery [107–109] or block copolymer gels in tissue engineering [110]. Finally, it is also worth recalling that the recent development of new synthesis strategies [1–4] has substantially increased the variability and scope of application of block copolymer materials. However, testing all possible variants for all their material properties, only through experimental means, is undoubtedly highly ineffective. In this regard, new theoretical approaches can provide valuable guidance and can become a major prerequisite on the route of target-oriented development of functionalized polymer materials. Therefore, our goal in this chapter will be to present new theoretical approaches, which are able to predict the structural–dynamical properties of the block-copolymer-based TPEs introduced previously.

3.1 Theory and simulation of block copolymers—state of the art

Despite these obvious needs, progresses in the theoretical prediction of material properties of block-copolymer-based TPEs have only been slow in the past [111,112]. Some of the major difficulties are summarized in the following: (1) their relaxation and, as a consequence, their equilibration is very slow, which renders the direct application of particle-based simulation methods, like e.g. MD, difficult [31]; (2) multiple length and time scales generally strongly influence their physical properties and must be taken into account, when overall thermodynamic and mechanical properties wish to be determined [12]; (3) the effect of the interphases on the physical properties is still not well understood and characterized [113]. As a result, their role is often neglected in the development of new theoretical approaches or it is included in a very empirical way [114]; (4) nonlinear external perturbations can damage the structure, which may lead to an uncharacterized new morphology that changes with time as further

deformation is exerted and/or healing does take place [111]; (5) the individual phases in such multiphase materials are not shaped or oriented as in the idealizations of simple analytical or numerical models, and several types can coexist [111]. Some efforts have been invested in the last few years to develop new simulation methodologies, partially addressing the difficulties previously mentioned [31,45–47,115,116]. For example, Aoyagi et al. [31] tackled the problem of slow equilibration of block-copolymer-based TPEs by generating equilibrated configurations with SCFT and using them as input for subsequent MD simulations. In this way they were able to study the deformation behavior of various triblock copolymer TPEs at the atomistic level. In another work Terzis et al. [45–47] developed a promising simulation strategy, which connects a coarse–grained description of entangled polymer networks with a kinetic Monte Carlo algorithm, to model the fracture deformation of multiphase polymer materials on the mesoscopic level of description. This approach allowed them to successfully simulate the damage of a polypropylene/polyamide6 interface in real time. We will demonstrate in the following that in the linear regime of mechanical perturbation a fully atomistic simulation is not necessary and a continuum-based FE method is enough to reproduce the linear mechanical properties within the experimentally available accuracy. By contrast, in case of the nonlinear regime, we will see that atomistic MD simulation methodologies are not suitable to predict the equilibrium mechanical properties of TPEs. This is due to the fact that block-copolymer-based TPEs relax their stress on the order of microseconds to seconds using various relaxation channels, like e.g. the self-retraction of dangling chains causing a power-law stress decay. In such cases novel MSM techniques are needed, which permit to suitably incorporate their relaxation mechanisms, taking place at different scales, and allow to model their slow relaxation to equilibrium.

3.2 Linear mechanical properties

In the following let us first focus on the study of the nature of linear elasticity in block copolymer-based TPEs, which is to date still not fully understood. To address this issue, we make use in our work in Ref. [54] of analytical and numerical approaches on the continuum-level of description, to investigate the linear elastic properties of a TPE composed of symmetric poly-(styrene–butadiene–styrene) (SBS) triblock copolymers forming PS phases with cylindrical morphology. Because of its technological relevance, extensive efforts have been invested to study its mechanical properties experimentally [55,117–119]. However, despite of that still only little is known about the interplay of the core nanophases and the importance of the molecular details in the material under deformation. For instance, a particularly interesting, as yet unsolved, question is the contribution of the confined elastomeric phase to the overall mechanical behavior and the question, whether an explicit resolution of the chains is necessary, to describe the overall mechanical behavior in the linear regime. In preceding theoretical studies Arridge and Folkes [117,119] predicted a rather untypical Poisson's ratio of $\nu_{PB} = 0.37$ for the confined PB phase by employing experimentally determined mechanical properties in conjunction with analytical continuum-based theories of fiber-reinforcement. By contrast, in bulk rubber materials the Poisson's ratio is

typically known to be at $\nu = 0.5$, which characterizes an incompressible medium. Arridge and Folkes explained this unusual finding with the argument that the PB bridging chains between the PS blocks might be too short and not sufficiently entangled, to exhibit typical rubber-like behavior. This would indicate that molecular characteristics are relevant, to reproduce the mechanical behavior of this SBS material in the linear regime of mechanical properties. In order to elucidate these interesting issues, we make use of the FE route and investigate the effectiveness of the numerical continuum-based approach in predicting its linear mechanical properties. We compare the obtained results with results from experimental measurements and various analytical continuum-based approaches, conceived for fiber-reinforced materials and employed in a previous work by Arridge and Folkes [117]. A brief summary of the analytical continuum-based methods, discussed in this section, is given in the following:

1. *Variational method* of Hashin and Hill [58,59] relies on an extension of the approach of Hashin and Rosen [60]. It employs the energy theorems of classical elasticity, to obtain upper and lower bounds for the five elastic constants. The minimum complementary energy theorem yields the lower bound, while the minimum potential energy theorem yields the upper bound. Hill [59] showed by formal and physical arguments that these are the best bounds that can be obtained without taking into account molecular details.
2. *Variational method* of Rosen [61] is an improvement of the composite-cylinder-assemblage model proposed by Hashin and Rosen [60]. This model incorporates randomness in size and structure of the fibers and permits the derivation of simple closed form expressions for the effective elastic moduli.
3. *Exact-calculation* method of Van Fo Fy and Savin [62] relies on Fil'shtinskii's approach for the treatment of fiber-composite materials [63]. It is based on the solution of the equations of elastic equilibrium using an expansion in elliptic functions, to solve the problem of hexagonal symmetry.

In this context it is also worth mentioning that the previous analytical theories have originally been designed for composite materials with inclusions, embedded in ordinary solid matrices with Poisson's ratios <0.4, and that they rely on several more or less controlled approximations. On the contrary, the FE route is accurate in principle, i.e. in the limit of an infinite number of elements the predictions must become exact. Within this approach, however, it is important to take into account that the rubbery phase is nearly incompressible and, thus, possesses a Poisson's ratio close to $\nu = 0.5$. A well-known difficulty in handling incompressible media with FE methods is that the standard displacement formulation of elastic problems fails and, typically, leads to highly oscillatory results, when the simple linear approximation with triangular elements is used [51]. In practice, the problems already arise when the material is nearly incompressible at $\nu > 0.4$. To overcome the difficulty, we employ the mixed finite-element (MFE) approach using a two-field formulation, where the displacements and the pressure are the free variables of the problem. Such a formulation allows the treatment of fully compressible phases as well as nearly incompressible ones, as they occur in the SBS TPE material considered herein.

Following the procedure of Arridge and Folkes [117], we adjust in our work in Ref. [54] the bulk and shear moduli of the model under consideration to match specific

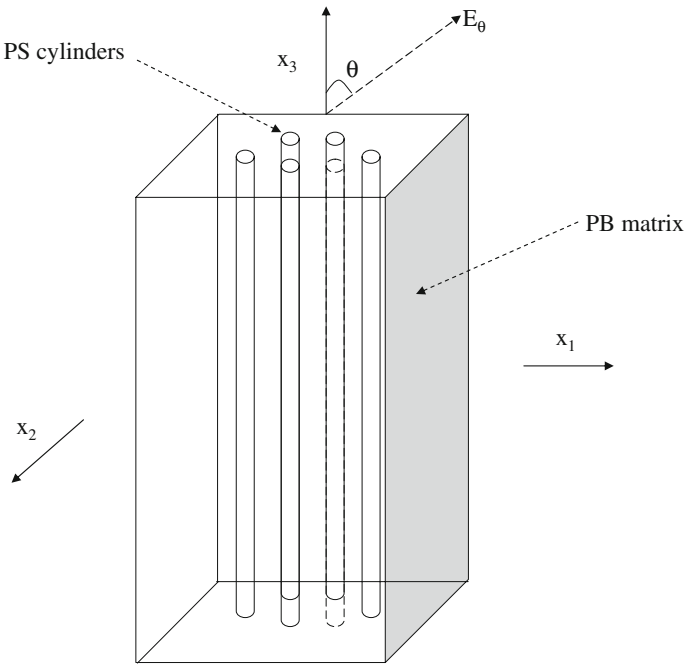

Fig. 2 Simulation cell of SBS material with cylindrical morphology

compliances with the experiments and, then, compare the calculated values of the remaining compliances among the various theories. The system under investigation is a SBS copolymer material with a weight fraction of 25% of PS. It is characterized by a hexagonally packed array of PS cylinders embedded in a matrix of PB, as visualized in Fig. 2. From the figure, it can easily be concluded that the system possesses hexagonal symmetry about the x_3-axis, which implies that the compliance tensor is symmetric about the leading diagonal and contains five independent compliance components S_{11}, S_{33}, S_{12}, S_{13} and S_{44}. S_{11} and S_{22} are, respectively, the compliances along the x_1- and x_2-directions, which are transverse to the fiber direction x_3 and equal due to symmetry. S_{33} is the component of the compliance tensor along the x_3-direction, while S_{44} is a shear compliance directly related to the shear modulus G_{SBS} of the model via $S_{44} = 1/G_{SBS}$. To test the reliability of the different theoretical approaches introduced previously, we compare the components of the compliance tensor obtained with the MFE method to the theoretical as well as experimental results presented by Arridge and Folkes in Ref. [117]. In particular, we consider the orientation-dependent compliance

$$S'_{33} = \frac{1}{E_\theta} = S_{11} \sin^4\theta + (2S_{13} + S_{44}) \sin^2\theta \cos^2\theta + S_{33} \cos^4\theta, \qquad (24)$$

where the angle θ is defined as shown in Fig. 2. In Fig. 3 we plot this quantity as a function of the angle θ. We deduce from the figure that the numerical continuum-based method, based on the MFE approach, and the analytical continuum-based method of Van Fo Fy and Savin provide reliable results, while other

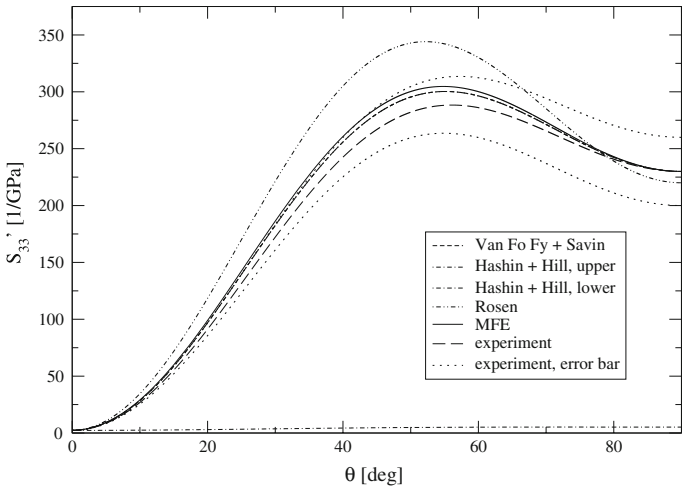

Fig. 3 S'_{33}-compliance yielded with the MFE method in comparison to the results obtained with the theories of fiber-reinforcement and the experiment. The compliances S_{11} and S_{33} are adjusted to the experimental results

analytical continuum-based theories are less valuable. As a consequence, we conclude that the description at the continuum level is accurate and that no detailed molecular information beyond the nanoscale morphology is needed to reproduce the experimental data in the linear regime of mechanical properties within the accuracy of the experimental measurements. Moreover, our investigation also indicates that the anomalous Poisson's ratio of the PB phase of 0.37, determined by Arridge and Folkes and attributed to molecular characteristics of the PB phase, is likely to be related to sample end effects arising in their mechanical experiments. In opposition to their results we show that the PB phase exhibits a typical nearly incompressible rubber-like behavior. Finally, our work in Ref. [54] also unambiguously demonstrates that a concerted improvement of experimental and theoretical techniques is necessary to gain a deeper insight in the small-strain behavior of block-copolymer-based TPEs.

3.3 Nonlinear mechanical properties

To explore the nonlinear regime of mechanical properties, we introduce in the following an analytical and numerical MSM approach. They are both employed to explain and predict the peculiar stress relaxation behavior of the block-copolymer-based TPE poly-(styrene–butadiene–styrene) (SIS) at long times, subjected to a nonlinear extensional strain.

3.3.1 Analytical multiscale-modeling approach

Among many challenges, the prediction and understanding of the stress relaxation behavior is of particular importance, because it provides informations about the molecular mechanisms affecting the macroscopic properties of materials. In case of TPEs

the stress relaxation behavior at long times has been studied in several experimental investigations [120]. Chasset and Thirion [121] recognized that an excellent representation of their data at times $t \gg \tau_p$ is given by a power-law equation of the type

$$E(t) \approx E_{t=\infty}\left[1 + (t/\tau_p)^{-\gamma}\right], \tag{25}$$

where $E(t)$ is the isothermal relaxation modulus. The parameter $E_{t=\infty}$ is the equilibrium modulus, while τ_p and γ are simple material parameters. In this context, it is worth mentioning that the first two parameters depend on temperature and crosslink density of the material [122–124], while the latter does not [125]. Ferry [122,123] has speculated that the molecular processes associated with the power-law decay are related to the relaxation of loops and free dangling chains, attached to the crosslinks of the polymer network. He assumed that their relaxation is slow because of the presence of entanglements, which act as topological constraints. This picture has been confirmed in the later theoretical studies of Curro and Pincus [122–124]. However, from stress relaxation experiments with various TPEs it is well-known since decades that, above a characteristic temperature T^*, deviations from power-law behavior can be observed after long times [20,120]. In the early 1970s Smith [120] concluded from his experiments on SBS TPEs that the deviations are due to plastic flow and breakup of the domains, which he presumed to be relatively soft at these temperatures. In a recent work Hotta et al. [20] deduced from their experimental investigations that their SIS TPEs undergo a stretched-exponential stress relaxation of the type

$$E(t) \approx E_{\tau_s\to\infty} \exp\left[-(t/\tau_s)^{\beta}\right], \tag{26}$$

where $0 < \beta < 1$ and τ_s are constants, while $E(t)$ is the time-dependent effective extensional modulus, defined through the stress–strain (σ–ϵ) convolution integral as

$$\sigma(t) = \int E(t - t')\frac{d\epsilon(t')}{dt'}dt'. \tag{27}$$

Moreover, $E_{\tau_s\to\infty}$ is the modulus in the limit $\tau_s \longrightarrow \infty$. They suggested that the stretched-exponential stress decay could be the result of a readjustment of the network, taking place via a rearrangement of the bridging chains. Relaxation phenomena, obeying a stretched-exponential decay law, have been found in several relaxation processes, such as e.g. in the relaxation of polymer glasses or gels [126]. Their occurrence is generally attributed to the presence of a disorder or/and strong interactions in the system, which lead to a superposition of different exponential processes or a superposition of intrinsically non-exponential processes. For instance, in Ngai's approach [127] the relevant network units relax independently obeying an exponential relaxation at times $t < t_c$, where t_c represents a characteristic crossover time. At $t > t_c$, these units undergo a transition to a relaxation of stretched-exponential-type due to strong interactions with neighboring units, causing a constrained motion and, therefore, a slowing down of the relaxation. In a recent paper Gurtovenko and Gotlib [126] demonstrated that a stretched-exponential decay in an inhomogeneously crosslinked network may also be the consequence of a broad size distribution of non-interacting

network regions, each composed of a certain number of relaxing elements (crosslinks, polydisperse chains, etc.). According to their approach, the phenomenon is the result of structural heterogeneities in the polymer network, which cause a superposition of the relaxation processes of the different domains in the network. These inhomogeneities may, e.g., arise by applying a mechanical deformation on polymer films or gels [128,129]. In such cases agglomerations of crosslinks are created and form domains, in which the crosslinks function as the relaxing elements and their respective numbers determine the individual contributions of the domains to the overall relaxation process.

In our work in Ref. [12] we investigate the possibility of a stretched-exponential decay behavior of the relaxation modulus in a homogeneously crosslinked network with transient crosslinks, which forms domains of different number of crosslinks above a characteristic temperature T^* but below the glass transition of the crosslinks, while subjected to a nonlinear tensile deformation. To this end, we develop an analytical MSM approach based on the approach of Gurtovenko and Gotlib, in which two different types of relaxing elements of the network contribute to the stress relaxation of the system, i.e. at short length and time scales the dangling chains and loops attached to the crosslinks, while at larger scales the crosslinks themselves. To describe the model in more detail, let us in the following regard a crosslinked polymer as an ensemble of network regions (domains), each having a finite number n of crosslinks (relaxing elements). In Fig. 4 we show a sketch of the network domains in case of a SIS copolymer material with spherical morphology in the range above the characteristic temperature

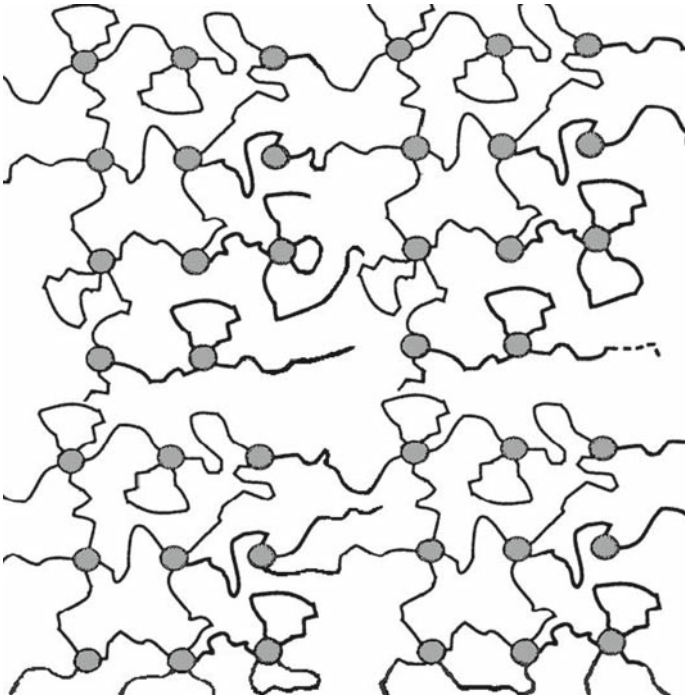

Fig. 4 Domains formed in a SIS copolymer material at temperatures above the characteristic temperature T^*, under a nonlinear tensile deformation

T^* but below the glass transition temperature of the PS crosslinks. In this regime the PS crosslinks are in a state of transient hardness, which causes that under the action of a nonlinear deformation and thermal fluctuations some of the bridging chains can pull out of the PS crosslinks. As a result, the system splits reversibly in crosslinks domains of different sizes, whose boundaries are determined by the chain pullouts. Inside the domains the network consists of a regular arrangement of PS spheres, interconnected by bridging chains of PI. On the junctions, free dangling chains and loops are attached, responsible for the slow power-law decay inside the domains at short time scales. As a consequence, within each domain we suppose a power-law relaxation of the following type:

$$E(t,T) = E_{t=\infty}(T)\left[1+\left(\frac{t}{\tau_0(T)}\right)^{-\gamma}\right], \tag{28}$$

where $\tau_0(T)$ characterizes the minimal relaxation time of the domain [122,123]. Similarly as in Eq. 25, the parameter $\gamma > 0$ represents the power-law exponent, which can easily be obtained from short-time stress relaxation experiments or numerical calculations. In our work in Ref. [12] we get the power-law coefficient γ from short-time stress relaxation measurements at temperatures below $T < T^*$ [20]. Since all the domains, of crosslinks consist of the same type of relaxing elements and have identical internal architecture, the minimal relaxation time at a given temperature can be considered to be similar for all the domains. For a time $t > \tau_{max}(n,T)$, it can now easily be demonstrated that, due to the finite number of relaxing elements, the stress relaxation of each domain goes over from the power-law relaxation in Eq. 28 into an exponential-relaxation law of the following type:

$$E(t,T,n) \approx E_{t=\infty}(T)\left(1+\frac{\gamma}{n}\left(\frac{\tau_{max}(n,T)}{t}\right)\exp\left[-\left(\frac{t}{\tau_{max}(n,T)}\right)\right]\right), \tag{29}$$

where $\tau_{max}(n,T)$ separates network motions of different scales, i.e. the relaxation of free dangling chains and loops at short times and the crosslinks at longer times. Let us next focus on the long-time viscoelastic behavior of our crosslinked polymer by determining the overall relaxation modulus of an ensemble of network domains, each relaxing according to Eq. 29, at long times. In the following we will refer to this model as the *domain model*. We suppose that the domains distinguish themselves only by their different number of crosslinks, which are embedded in an effective viscous medium common for all the domains, and that, due to thermal fluctuations, they undergo reversible fluctuations in the domain sizes via a permanent network readjustment. Moreover, we assume in a first approximation that the network domains relax independently of each other with characteristic relaxation times and that the domain sizes are distributed according to a Gaussian probability distribution function, derived from the equilibrium fluctuation theorem [130]. It can easily be shown that, under such conditions, the overall relaxation modulus of an ensemble of domains obeys a stretched-exponential law of the following type:

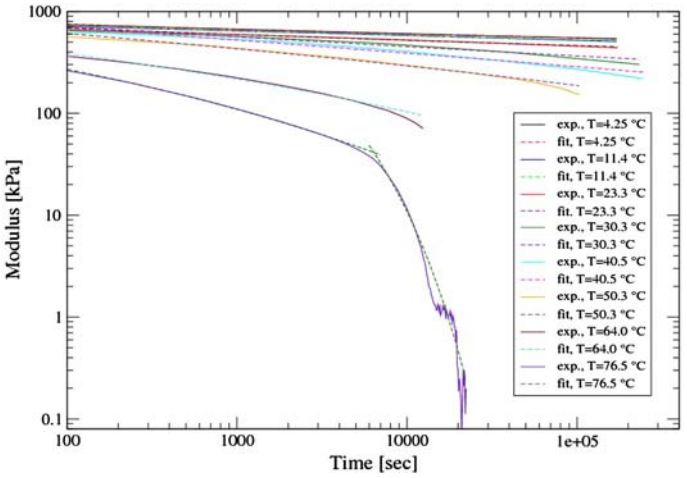

Fig. 5 Experimentally and theoretically determined effective extensional modulus versus time at different temperatures for the SIS material with 14% PS, where PS spheres with cubic phase symmetry are embedded in a PI matrix

$$E(t,T) \approx E_{t=\infty}(T)\left[1+\frac{C_1}{\langle n\rangle}\left(\frac{t}{\tau^*(T)}\right)^{\frac{(\sigma-3)}{(1/\gamma+2)}}\exp\left(-\left(\frac{t}{\tau^*(T)}\right)^{\frac{2}{(1/\gamma+2)}}\right)\right], \quad (30)$$

where $\tau^*(T)$ is a characteristic relaxation time, determining the stretched-exponential decay, and C_1 is a constant.

To assess the usefulness of our analytical multiscale model, we make use of our derived relaxation law in Eq. 30 by fitting it onto the experimental measurement results of Hotta et al. [20]. In Fig. 5 we visualize the theoretically and experimentally determined extensional modulus versus time at different temperatures obtained for the SIS material with spherical PS morphology. We see that our domain-model approach qualitatively correctly reproduces the experimental curves at all temperatures. In particular, we observe that our approach correctly predicts the power-law decay behavior, experimentally observed by Hotta et al. below a characteristic temperature of $T^* \approx 303\,\mathrm{K}$, by assuming a macroscopically large single-domain system of crosslinks. With increasing temperature, our single-domain system splits reversibly in a broad size distribution of domains and undergoes fluctuations in the domain sizes via a permanent network readjustment. These domain size fluctuations are induced by thermal fluctuations, causing fluctuations of stresses on a local scale. Regarded from a molecular perspective, the stresses on the bridging chains decrease the activation barriers for the chain pullouts, making them in this way more likely. By further taking into account that the relaxation moduli of the different domains obey an exponential decay law inside the domains at long times according to Eq. 29 and superimpose as an ensemble, our approach correctly predicts the stretched-exponential relaxation law of Eq. 30, which governs the decay behavior of the overall system above T^*. The deviations observed at longer times announce the beginning of the terminal relaxation zone. In this regime only the single domain still needs to relax, which

possesses the largest number of relaxing elements and the longest relaxation time. As a consequence, it determines the final relaxation behavior via the exponential given in Eq. 29, and the overall relaxation modulus decays exponentially to zero, since at this stage no superposition is possible anymore. We draw similar conclusions by applying our model to TPEs with different composition and morphologies [12,131]. Further experimental evidences for the process of chain pullout and the resulting readjustment of the transient network under deformation are in particular the persistent change of sample length after unloading and the recovery of the original sample size at long times and/or upon annealing [20,132]. In conclusion, our analytical multiscale analysis confirms the importance of the chain-pullout mechanism in the stress relaxation process of TPEs and demonstrates the involvement of multiple length and time scales in their nonlinear mechanical behavior. Moreover, in the following we will see that it also delivers important information about the nature of the glassy state in multiphase and pure polymer materials. To investigate these issues in more detail, we introduce in the subsequent sections a new glass transition theory as well as a numerical MSM approach, which will provide a conclusive explanation for the transient hardness of the PS crosslinks and elucidate the important role of the interphase regions in the stress relaxation of these materials.

3.3.2 Numerical multiscale-modeling approach

Since the early 1970s, it is well-established that the properties of the core nanophases in block-copolymer-based TPEs considerably affect their overall mechanical properties and, thus, their appropriate treatment is a crucial issue in the development of new calculation tools. However, several recent experimental studies have clearly demonstrated that, besides the correct handling of the core nanophases, an adequate treatment of their interphases is another major challenge one has to face on the way of target-oriented design of these materials. For instance, Diamant et al. [111] concluded from their tensile tests with TPEs composed of various phase-separated styrenic block copolymers that a linear or nonlinear mechanical perturbation leads to a stress concentration, localized in the interfacial region between hard and soft nanophases, and that the impact of the interfacial region on the overall mechanical properties becomes increasingly important with increasing mechanical perturbation imposed on the system. Moreover, they found that, if the interphase is diffuse with a small composition gradient, the domains are not in register and they fail individually, which explains that macroscopic yielding cannot be observed in such systems. In contrast, if the composition profile has a sharp gradient, high local stress concentrations are generated at the interphases, which causes that under a nonlinear strain all domains fail together in a cascade. In a later study Henderson and Williams analyzed the issue of composition profiles at block copolymer interphases using experimental and theoretical approaches [133,134]. They showed that phase-separated block copolymers generally possess asymmetric interphases, caused by a partial enrichment through one of the components. Morèse-Séguéla et al. [135] deduced from their DSC and 13C-NMR-line-width measurements on low-molecular weight PS-PI diblock copolymers that at the interphases there are strong dynamical interactions between the chain segments in the soft and hard nanophases. They deduced that these interactions are responsible for

the abnormal decrease of the glass transition temperature T_g at the interphases, instead of the mixing of the two components assumed in previous works [136,137]. In a later study Stoeppelmann et al. [138] have shown evidences for an asymmetric density and motional profile of the chain segments at the interphases, using 2H-nuclear-magnetic-resonance spectroscopy. Very recently, Huy et al. [139] proposed that the interphases of tapered block copolymers can act as stress absorbers, which allow a more uniform stress distribution. In conclusion, all these experimental works indicate that the study of the structural–dynamical processes of the chain segments at the interphases are an important issue and their consequences on the macroscopic physical properties need to be better understood. To mimic their behavior, we have devised and applied a new numerical MSM procedure based on the combination of a modified SCFT approach and a kinetic Monte Carlo (KMC) method, which will be discussed in the following.

3.3.2.1 Structural–dynamical model To develop our numerical MSM approach presented in the subsequent section, we formulate and study in our work in Ref. [140] a new glass transition theory, which is capable to describe the transient nature of the PS crosslinks in styrenic TPEs above the characteristic temperature T^* and, thus, to explain their peculiar stress relaxation spectrum as well as viscoelastic behavior. In our analytical multiscale model, introduced in Sect. 3.3.1, we have assumed that the crosslink domains are formed as a result of a structural–dynamical process, involving the readjustment or pulling of the PS blocks out the PS crosslinks. This process is thermally activated in nature and implies a non-singular viscosity in the glassy crosslinks, allowing a certain mobility of the PS blocks under the action of strain. A further important implication of this process reveals itself in the transition from Williams–Landel–Ferry (WLF) to Arrhenius behavior of the mechanical shift factors, while passing through T^* from below. In Fig. 6 we show the logarithm of the shift

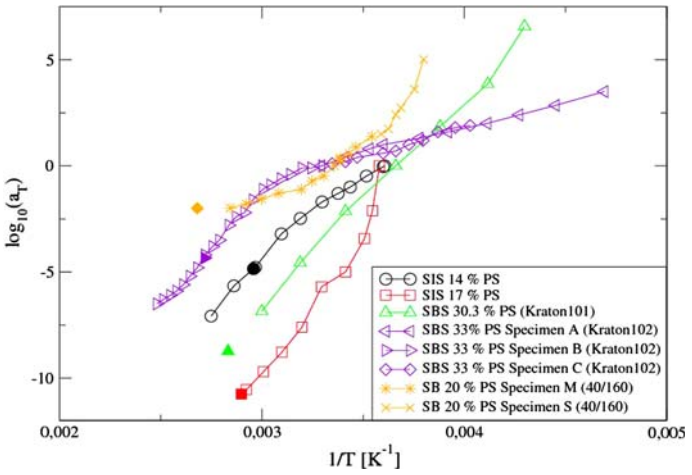

Fig. 6 Logarithm of the shift factor versus inverse temperature obtained from stress relaxation experiments with different phase-separated styrenic triblock and diblock copolymer materials. Filled symbols with the same color designate the respective T_g's of the PS phases

factor versus inverse temperature, obtained from various mechanical experiments with different styrenic triblock TPEs. We compare these shift factors with values obtained by Morton et al. [131], using a diblock material composed of poly-(styrene–butadiene) (SB) copolymers. The transition in behavior of the shift factors from WLF- to Arrhenius-type with decreasing inverse temperature can be explained in the following way. At and above $1/T^*$, the PS crosslinks are fully rigid and the mechanical behavior of the TPEs is dominated by the relaxation of the dangling chains, attached to the crosslinks, and, thus, the shift factors obey a WLF equation with reference temperature T_r,

$$\ln a_T = -\frac{C_1(T - T_r)}{C_2 + T - T_r}, \tag{31}$$

where the constants $C_1 \propto 1/C_2$ and $C_2 = (T_r - T_2)$. With decreasing inverse temperature, we observe that the curves of the triblock TPEs progressively become linear, approaching $1/T_g(PS)$. This behavior is well-reproduced by the Arrhenius law given by

$$\ln a_T = -\frac{C_3}{RT} + C_4, \tag{32}$$

where C_3 and C_4 are time-dependent constants. Moreover, we notice that in the linear regime all triblock TPEs adopt the same slope, which indicates that at this stage phases of the same chemical composition, i.e. the PS crosslinks, predominantly contribute to the stress relaxation of the TPE materials. Next, further passing through the glass transition temperature of the PS crosslinks, leads to an additional crossover in behavior of the shift factors from Arrhenius- to WLF-type, as can be deduced from Fig. 6 for the TPE Kraton102. Afterwards, we compare in the same figure the triblock TPE results with the ones from the diblock copolymer material. We observe that the diblock curve does not show the Arrhenius-type behavior of the shift factors and conclude that the relaxation of the diblock material is not dominated by a thermally activated process in the temperature range under consideration. As a result, we infer from our theoretical investigation that a rate-determining thermally activated process determines the behavior of the glassy crosslinks in styrenic triblock TPEs in the temperature range $T^* < T < T_g(PS)$, which is in consistency with several experimental observations [20,120]. In our work in Ref. [140] we find this process to be related to the thermally activated breaking and re-forming of vdW bonds. Moreover, we identify the characteristic temperature T^* to be identical with the second-order equilibrium transition temperature T_2 of the glassy PS phases, postulated by Gibbs and Di Mario in the 1950s to avert the entropy crisis in the thermodynamic formulation of their glass theory [141–143]. Based on these observations, we combine in our work in Ref. [140] the recently introduced theory for glasses of Di Marzio and Yang [144] with the significant-structure theory of Eyring and Ree [145,146], and formulate a new glass theory, which is capable to explain the characteristics of the mechanical behavior of the TPE materials discussed previously.

To introduce our glass model developed in Ref. [140], let us consider that a glassy polymer is the frozen state of an overcooled melt, which can spatially be decomposed in elementary units containing polymer chains held together by transient vdW bonds

[131]. In the following we will refer to these elementary units as activation units (AUs). Moreover, we assume that the thermally activated process, taking place within the AUs, is a yielding process, which may be described as a slip-shear motion involving the breaking and re-forming of vdW bonds. It is assumed to be the primary mechanism of deformation in the range of temperatures under investigation. In our theory for glasses we make use of a trapping description to describe this micromechanical process, in which escapes from deep energy wells provide the rate-determining steps. In Fig. 7 we show simplified sketches of the configuration space of our glass model in different temperature ranges, accessible within a typical experimental timeframe. The points represent configurations of AUs and the connecting lines represent allowed transitions between the configurations. Configuration points belonging to the configurational sea of shallow energy wells are denoted as N_j and those belonging to the deep energy wells as M_j. The horizontal lines with rates α_j for traveling to the right and β_{j+1} for traveling to the left designate motions of the configuration point among the configurational sea of shallow wells. The vertical lines connect the configurational sea to

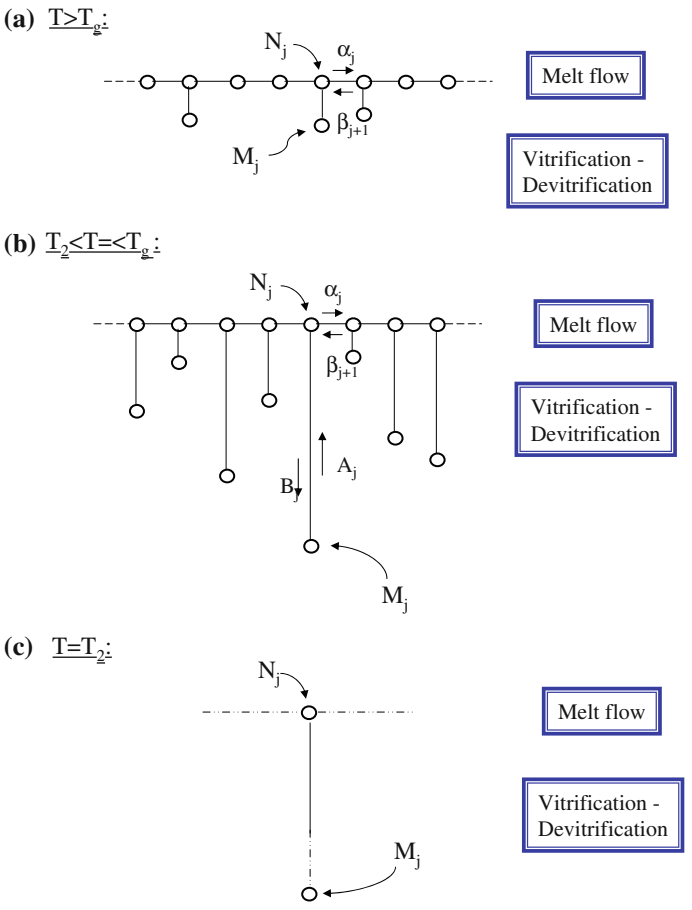

Fig. 7 Sketches of the underlying glass model in different temperature ranges

the deep wells by assuming that the length of each vertical line is proportional to the potential energy depth of the well. The rate of escape from the deep wells is given by A_j and the rate of capture by B_j. When the configuration point is in a deep well, there is no motion. In Fig. 7a we show the configuration space of the glass-forming material at a temperature somewhat above T_g. In this regime there are only a few deep wells relative to the number of shallow wells, and the energy difference between them is rather small. As a consequence, the configuration point migrates rapidly from well to well within the configurational sea of shallow wells, and the system is able to flow under the action of an external strain. In Fig. 7b the material is in the Arrhenius regime, characterized by the range of temperatures $T_2 < T \leq T_g$. In this situation a configurational sea of shallow energy wells coexist with deep energy wells, and it is assumed that the jumps out of the deep wells are the rate-determining steps. Under these conditions, the material is solid-like, but flows very slowly under the action of an external strain. If the configuration point is in one of the deep wells, it jumps out of it after a long period of time and wanders within the configurational sea of shallow wells, until it falls into another low-lying well. It then stays in this well for another long period of time until it jumps out of it, repeating the process all over again. The rate-determining step in this model is a simple vitrification/devitrification process without flow of matter, caused by the formation/breaking of transient vdW bonds. Motion involving flow of matter occurs only, when the configuration point has escaped and cruises around in the configurational sea of shallow wells, until it falls into another low-lying well. In Fig. 7c we see the material's configuration space at T_2. At this temperature, there is only one configuration remaining, which is infinitely deep in energy, and, thus, in this situation the trajectory is trapped in the deep well. In this regime the material has no freedom to rearrange and its viscosity diverges. Within this picture, the glass transition phenomenon can now be explained by the appearance of *non-equilibrium spatio-temporal fluctuations* slightly above the glass transition temperature, which lead to variations in the viscosity throughout the system and induces the creation of *solid clusters* in the polymer melt. At T_g, the system possesses the critical fraction of solid clusters with respect to the fraction of the melt-like regions, so that the solid clusters are able to connect to each other. This leads to the formation of a continuous rigid backbone, causing a sudden increase in the viscosity, and the system gets trapped in a *quasi-equilibrium state* by undergoing a *percolation transition*. Experimental evidences for the spatio-temporal heterogeneities in vicinity of T_g for glass-forming polymer melts have been accumulated over the past decade using experimental techniques, such as NMR, fluorescence recovery, dielectric hole burning or solvation dynamics [147,148]. By applying our glass model to explain the mechanical behavior of the styrenic TPEs discussed previously, we conclude that the occurrence of the Arrhenius regime relates to the large but only finite increase of the viscosity in the PS crosslinks at their glass transition temperature $T_g(PS)$, where a singular behavior is predicted by other glass models instead. In contrast, our glass model predicts a singular behavior of the viscosity at the characteristic transition temperature T^*, which we find to be identical with the equilibrium second-order transition temperature T_2, postulated by Gibbs and Di Mario in the 1950s [141–143].

Based on the glass model introduced previously, we propose in Ref. [131] an algorithm for the simulation of the slip-shear process, involved in the glassy crosslinks of

styrenic triblock TPE materials in the Arrhenius regime $T_2 < T \leq T_g(PS)$. It can be formulated as the following two-step procedure:

1. an AU is selected in space and the vdW bonds, acting between the styrene monomers within an AU, are cooperatively formed or broken through thermal activation, depending on whether the AU in its original configuration is in a melt-like or solid state. The thermally activated process is efficiently mimicked with a kinetic simulation algorithm;
2. under the action of strain, a subsequent step of flow motion of the chains within the melt-like (rubbery) phase is incorporated into the algorithm via minimization of the system's free energy.

An implementation of this two-step procedure and applications to the SIS TPEs, discussed previously, will be presented in the subsequent section.

3.3.2.2 Combined KMC–SCFT algorithm To simulate the structural–dynamical model introduced previously, we develop in Ref. [131] a numerical MSM approach, which

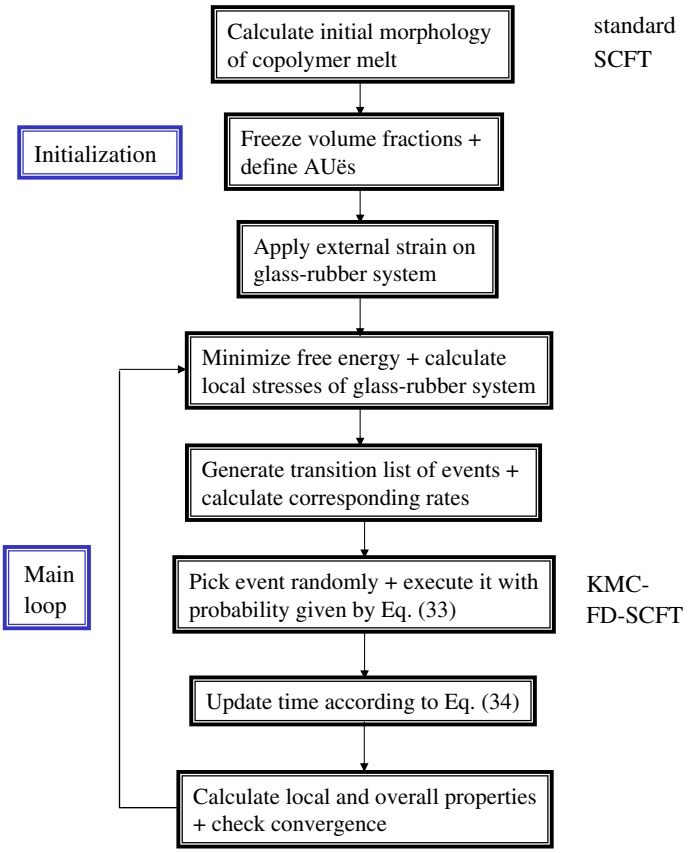

Fig. 8 Sketch showing the basic steps of the KMC–SCFT algorithm

directly couples a mesoscale SCFT approach on the chain level of description with a KMC algorithm, allowing to calculate the transition rates on the fly and to simulate the evolution of the system in real time. Its basic steps are visualized in Fig. 8. In the preliminary step we discretize the real space grid of the simulation cell in AUs and determine the initial configuration of frozen AUs in the system. This is achieved by minimizing the free energy of the copolymer melt and calculating its initial phase-separated structure using the standard SCFT approach [149], which provides initial fields and volume fractions of the styrene and isoprene monomers. The procedure delivers a fully relaxed and unstrained morphology, and the phases, designated as the glassy phases, can now be frozen by fixing their respective volume fractions locally. In a subsequent step an external strain is imposed and the partially frozen system is allowed to relax to mechanical equilibrium by minimizing its free energy $\tilde{F}$ with a constrained SCFT algorithm, which we call *frozen-domain* SCFT (FD-SCFT) algorithm. From this new configuration, the local stresses, fields and volume fractions on the grid are determined. Next, the KMC procedure is started by generating the list of possible transition events, $n = 1, \ldots, N$, for the given configuration of AUs $\{\lambda\}$ with stress distribution $\{\sigma\}$ and by calculating the transition rate, r_n, of each event n. The transition events are given by the AUs that can either be in a vitrified or devitrified state. In our approach we only allow the boundary AUs at the glass–rubber interfaces to contribute to the configuration space. AUs of the melt phase are allowed to undergo with a certain transition probability the vitrification process to become frozen AUs, while boundary AUs of the glassy phase are allowed to melt with a certain probability. Having generated the list of possible transition events, an event n is picked with probability

$$p_n = \frac{r_n}{\sum_{i=1}^{N} r_i}. \tag{33}$$

The selected event is executed and time is advanced by

$$\tau = \frac{\ln(\xi)}{\sum_{i=1}^{N} r_i}, \tag{34}$$

where ξ represents a random number generated from a uniform distribution in the range (0,1). Flow in the rubbery phase is allowed in a subsequent step through minimization of the free energy, which permits the rearrangement of the polymer chains. From this new configuration, the local and overall properties are determined. At this stage, it is also important to mention that equilibration through minimization is performed after each KMC step, since molecular rearrangements of the chains in the rubbery phase are much faster than the relaxation processes, taking place in the glassy phase. Finally, in the last step the convergence with respect to the local and overall properties are checked.

To assess the usefulness of our combined KMC–SCFT approach, we perform calculations for a lamellar TPE material composed of SIS triblock copolymers with alternating glass–rubber phases, subjected to an extensional strain of 8.3%. For the calculations, we use average volume fractions for the styrene and isoprene monomers of $\bar{\phi}_{S|I} = 0.5$, a Flory–Huggins parameter of $\chi = 0.2$ and a polymerization index

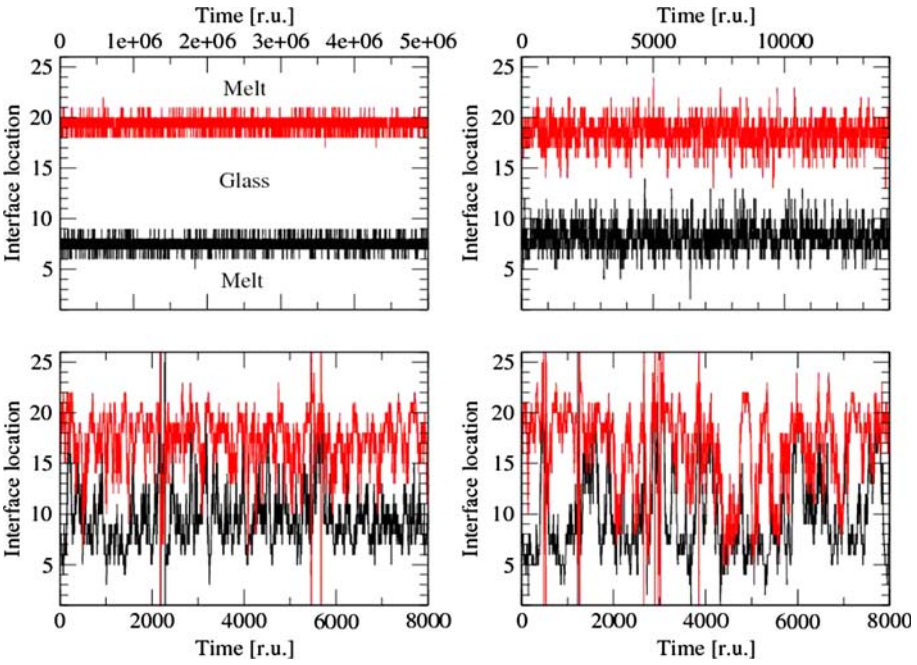

Fig. 9 Glass–rubber interface locations versus real time at various temperatures for a lamellar TPE material composed of SIS triblock copolymers, determined with the combined KMC–SCFT algorithm. In the calculations the following temperatures have been considered: $T = 305\,\mathrm{K}$ (upper left), $T = 320\,\mathrm{K}$ (upper right), $T = 350\,\mathrm{K}$ (lower left) and $T = 380\,\mathrm{K}$ (lower right)

of $N = 100$, as well as a lattice spacing of $dx = 0.1 R_g$. In Fig. 9 we visualize the resulting fluctuations of both glass–rubber interfaces as a function of real time at 4 different temperatures, i.e. $T = 305$, 320, 350 and 380 K, where the first 3 temperatures lie below $T_g(PS)$. From the graphs, we deduce that the interfaces at the first 3 temperatures fluctuate about their equilibrium average values and that the magnitude of the fluctuations, as well as the frequency of events, within a time interval grow with increasing temperature. The latter behavior can easily be explained physically by the increase of the transition rates for the processes of breaking and re-forming of the vdW bonds in the glassy phase, as the kinetic energy in the system becomes larger. At $T = 380\,\mathrm{K}$, we observe that the interface locations do touch each other and that, as a consequence, the glassy phase of PS is completely molten above its glass transition temperature. Next, in Fig. 10 we show the 1000-point moving averages of the interface locations versus the rescaled real time at different temperatures. For a better visualization, we rescaled the time of the curves according to the following equation $t' = A_t(T)t$, where t' represents the rescaled time and $A_t(T)$ the scaling factor. The scaling factors are $A_t(T = 307\ K) = 32$, $A_t(T = 310\ K) = 135$, $A_t(T = 320\ K) = 375$, $A_t(T = 330\ K) = 480$ and $A_t(T = 350\ K) = 665$. We recognize that with increasing temperature the fluctuations become stronger and the glassy phase between both interfaces in average becomes narrower. The latter behavior relates to the fact that the glassy phase melts progressively due to the gradual change of the

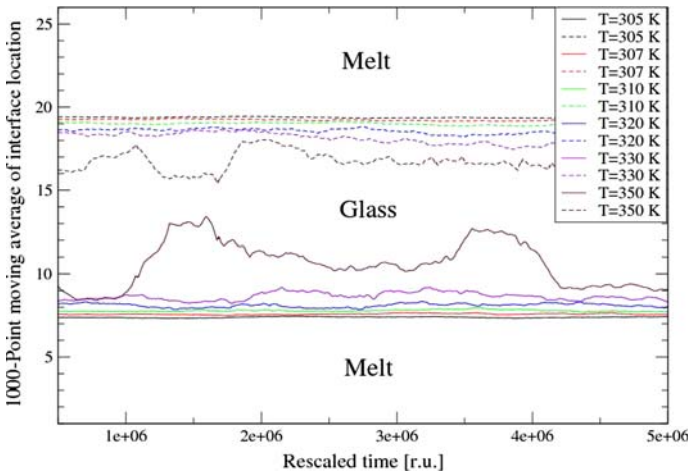

Fig. 10 1000-point moving averages of the interface locations versus rescaled real time at different temperatures for a lamellar TPE material composed of SIS triblock copolymers, determined with the combined KMC–SCFT algorithm

composition profile. These results are in consistency with a series of experimental investigations from the late 1960s and early 1970s [120,150,151], from which it has been inferred that with increasing temperature the PS crosslinks in styrenic TPEs become softer. In these works a higher ductility of the PS glassy phase was reported at lower temperatures, than predictable from the values of the bulk material. Moreover, in a recent experimental study of Park et al. [152] thickness and composition dependence of the glass transition temperature in thin random copolymer films was observed. Next, we deduce from Fig. 10 that, approaching the glass transition temperature of the crosslinks from below, there is an increased probability that the crosslinks melt for a short period of time, due to fluctuations. We can particularly well conclude this from both interface curves at a temperature of $T = 350\,\mathrm{K}$. We see that, in the time interval between $t' = 1 \times 10^6$ and $t' = 2 \times 10^6$, the curves do almost touch each other and we can safely predict that, if we would run the simulation for a longer time, instantaneous melting, due to fluctuations, would take place. In the following we refer to this phenomenon as *fluctuational melting* and emphasize that it has important consequences for the mechanical properties of these materials. This is due to the fact that, in the small time-frame the crosslinks are in the molten state, the chains can partially or fully pull out of the crosslinks under the action of strain and in this way relax their stress. In contrast, at a temperature of $T = 305\,\mathrm{K}$, we see that the interface curves are far apart and fluctuate only slightly. In this situation it is very improbable that they will coincide over some time interval and that fluctuational melting can take place, even in a simulation run of infinite time. As a consequence, at this temperature the glassy crosslinks remain rigid, and the material does not flow under the action of strain on a computationally as well as experimentally accessible time-scale. Note that, due to the restriction in computational time, we could not explicitly show such an instantaneous melting event here, but we plan to do extensive investigations on this phenomenon in a subsequent work. In Figs. 11 and 12 we show the resulting time-averaged internal stress as a function of the grid number at 2 different temperatures, i.e. $T = 305\,\mathrm{K}$ and

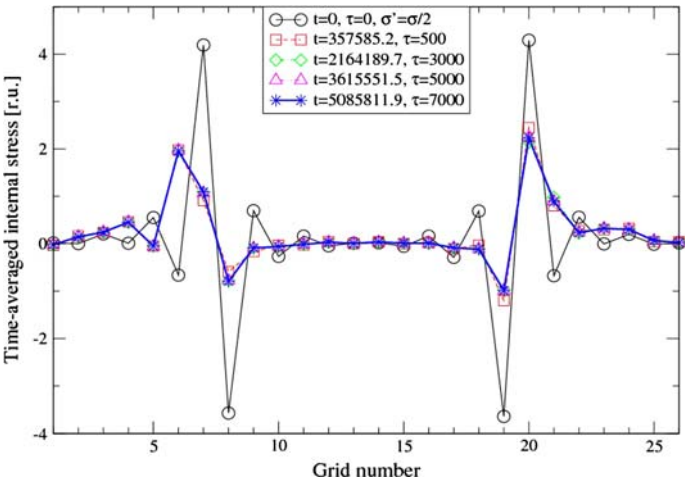

Fig. 11 Time-averaged internal stress as a function of the grid number for a lamellar TPE material composed of SIS triblock copolymers at $T = 305\,\mathrm{K}$, determined with the KMC–SCFT algorithm

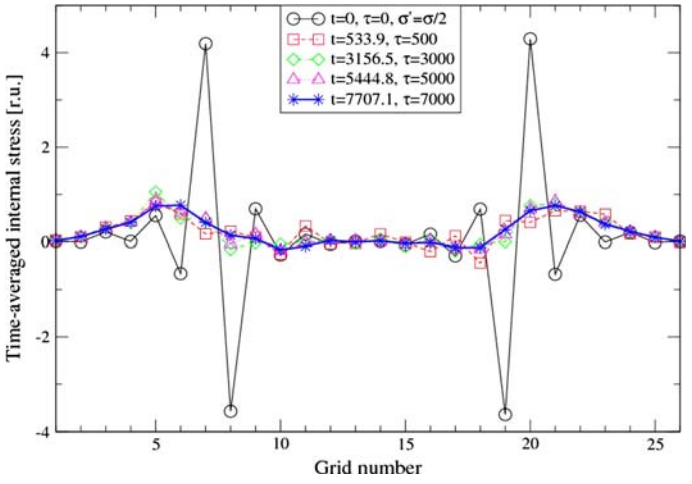

Fig. 12 Time-averaged internal stress as a function of the grid number for a lamellar TPE material composed of SIS triblock copolymers at $T = 350\,\mathrm{K}$, determined with the KMC–SCFT algorithm

$T = 350\,\mathrm{K}$ respectively. We compare the curves obtained with increasing time to the static internal stress configuration at $t = 0$, where no interphase dynamics is involved. For a better visualization, we rescaled the static stress curve as $\sigma' = \sigma/2$. It is worth mentioning at this stage that a stress concentration at static glass–rubber interfaces is a phenomenon one should expect from a physical point of view. Since the seminal work of Griffith in the early 1920s [153], it is well known that in materials with failures the stress is typically concentrated around the failure points. He recognized that, when a nominal stress is applied to the external surface of a brittle material, the actual stress at the flaw can be many times the value of the externally applied stress and it is typically amplified at the flaw's corner. In case of our glass–rubber system, calculated

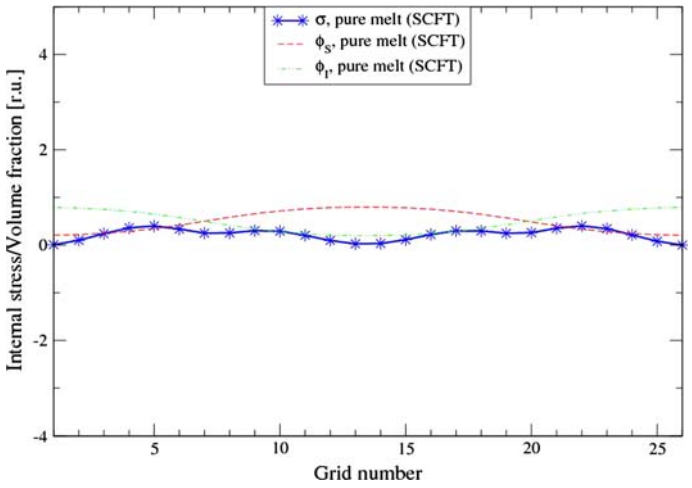

Fig. 13 Internal stress and volume fractions of the styrene and isoprene monomers as a function of the grid number for a lamellar melt-like system composed of phase-separated SIS triblock copolymers, determined with the standard SCFT algorithm

with the FD-SCFT algorithm, the stress concentration appears at the edges of *sharp* and *static* glass–rubber interfaces, as a result of an external mechanical perturbation applied to the system. By now further considering Fig. 11, we recognize that the time-averaged stress profile at $T = 305\,\mathrm{K}$, computed with our KMC–SCFT algorithm, still possesses a strong stress concentration at the interphases, even if the stress peaks are significantly reduced compared to the static internal stress profile at $t = 0$. We conclude from this observation that the structural–dynamical process is rather ineffective in reducing the stress concentrations at temperatures in vicinity to $T^* = T_2$, which can be explained by the low kinetic energy of the chain segments leading to an ineffective stress distribution over the interphases. Next, by comparing the time-averaged stress profile at $T = 305\,\mathrm{K}$ with the corresponding curve at $T = 350\,\mathrm{K}$ in Fig. 12, we deduce that the stress peaks significantly decrease in magnitude with increasing temperature, and that the double peaks at both interphases vanish and are replaced by single peaks. We also notice by considering the stress profiles at different times that the interphase dynamics causes a smoothing of the internal stress profile as the system evolves in time, which is due to the partial cancellation of the sharp and static internal stress configurations. At $T = 350\,\mathrm{K}$ the importance of the interphase dynamics becomes most apparent. The stress profile becomes almost similar in shape to the stress profile of the melt-like SIS system, computed with the standard SCFT approach [149] and shown in Fig. 13. Finally, it is also important to point out that our calculation results are supported by several theoretical and experimental investigations. The implausibility of sharp interfaces at such small scales together with the presence of interphase regions with mixed monomeric composition [154], motivated Leary and Williams to introduce the thick-interface concept, to model such materials [155,156]. In a later work Diamant et al. [111] deduced from their tensile tests on TPE samples that a linear or nonlinear mechanical perturbation provides a stress concentration, localized in the interfacial region between hard and soft nanophases. In a subsequent work Diamant

and Williams [157] explained the temperature-dependence of the recovery behavior of their TPE materials, subjected to a large nonlinear deformation, with the gradual change of the degree of vitrification with monomeric composition. Moreover, Huy et al. [139] concluded from their experiments with different tapered block-copolymer-based TPEs that a gradual composition profile permits a more uniform stress distribution at the interphases. They suggested that the interphases can be tuned to act as efficient *stress absorbers*, reducing the extent of the stress transfer between the core nanophases. In conclusion, from this study we retain that a suitable treatment of the interphase dynamics and morphology is crucial to model these materials adequately. Moreover, our investigation also provides an explanation and confirms the importance of the chain-pullout mechanism in the stress relaxation and viscoelastic behavior of block-copolymer-based TPEs.

4 Neutral and charged polymer solutions

Polymer solutions are polymers embedded in a solvent that are well-known to play a vital role in nature and technology [158,159]. They can be composed of neutral polymers, which possess no electrical charge or ionizable groups along their backbone and can be soluble in water or not. Examples are polyethylene oxide, cellulose, sugar, polyvinyl alcohol or polystyrene, among others. Their solutions have been extensively investigated in the past using various experimental as well as theoretical techniques, and their structures and properties are now well understood. Another type of polymer solutions consists of charged polymers, so-called polyelectrolytes (PEs). They are characterized by long polymeric chains, possessing a multitude of ionizable groups along their backbone that may dissociate in a polar solvent by producing charged species [160]. Among the most prominent examples are the nucleic acids DNA and RNA, which are highly charged biopolyelectrolytes controlling the development and functioning of living cells. In addition to their central role played in biological systems, PEs find widespread use as solubilizing agents, phase separation agents and rheological property modifiers in daily life and technological applications [161]. However, despite of their importance and in contrast to neutral polymer solutions, PE solutions are still only poorly understood [162,163]. This relates to the fact that their chemistry and physics is influenced by many controlling parameters, such as molecular weight, salt concentration, pH of the solution, etc. Another important characteristic of PE systems is the coexistence of long-range Coulomb and short-range excluded volume interactions. The presence of long-range interactions generally renders their simulation particularly difficult, because of the need for computationally expensive techniques, like the Ewald summation [25], for their appropriate treatment. Moreover, their often highly polymeric nature introduces additional complexity by severely slowing down their equilibration [34]. Finally, additional difficulties can occur in the computation of open PE systems at lower temperatures in the range of physical interest, because conventional grand canonical algorithms are known to become increasingly inefficient with growing interaction strength between the interacting monomers [37,90]. Since most PE systems, like e.g. living cells, are open systems where matter and heat

exchange between the system and its surroundings does occur, this represents a major drawback on the route towards understanding and predicting their physical properties.

4.1 Theory and simulation of polymer solutions—state of the art

Our good understanding of neutral polymers solutions is due to the fact that the range of interactions between the monomers is much smaller than the scale determining the physical properties of the solutions. As a result, fluctuations are reduced and the inter-monomer interactions mainly affect adjustable prefactors, rather than the exponents of the scaling laws. By contrast, PE solutions are controlled by an intricate interplay of short- and long-range interactions. The screening of the electrostatic interactions, i.e. the tendency of oppositely charged counterions to spatially arrange in such a way as to render the effective interactions between any like-charged monomers short-ranged, introduces yet another length scale in the problem, which may be comparable to the chain size or to the correlation length. However, as we will discuss more extensively in the further development, the distribution of counterions around the monomers limits not only the range of their effective interactions, but also implicates the renormalization of their charges as a result of counterion condensation. The screening process is influenced by the local chain architecture, which indirectly affects the long-range part of the interactions, and, therefore, has a nontrivial effect on the stiffness of the PE chains.

Most currently available theoretical approaches for treating neutral polymer and PE solutions are based on particle-based computer simulation techniques, like e.g. the conventional molecular dynamics (MD) [32] or Monte Carlo (MC) methods [164,165]. However, their inherent spatial and temporal limitations prohibit their straightforward application to systems with long polymer chains, characterized by slow equilibration times [33,34], like e.g. biopolyelectrolytes [30] or block-PE solutions [166,167]. To cope with these difficulties, we present in the following alternatives to the particle-based simulation methods previously mentioned, which rely on the field-theoretic formalism introduced in Chapter 2, and investigate their suitability in describing neutral and charged polymer solutions.

4.2 Concepts and methodologies

4.2.1 Beyond mean field methods

Since the pioneering works of Edwards [83] and de Gennes [168], it has been well-acknowledged that concepts originally introduced in quantum field theory (QFT) [94], like e.g. functional integrals or renormalization group theory, have substantially contributed to major breakthroughs in the field of polymer science [34,41–43,169]. For instance, the groundbreaking idea of Edwards to use functional integral methods, to investigate the physics of polymers and complex fluids, has led in the last few years to a rapid development of analytical calculation and computer simulation tools, suitable for describing structure and properties of a wide variety of important polymer systems, including polymer melts, blends and block copolymers, etc. [41–44,131,169–176].

This great success is, to a large extent, due to the introduction of the MF approximation, which has led to many important new physical insights into a broad class of polymer materials at rather low computational cost. However, as we already mentioned in Sect. 2.3, there are a multitude of cases for which the MF approximation provides inaccurate or even qualitatively incorrect results, like e.g. neutral and charged polymer solutions in dilute and semidilute concentration regimes [34]. In such situations the partition function integral defining the field-theoretic model is not entirely dominated by a single MF configuration and field configurations far from it can make important contributions, which require the use of more sophisticated calculation techniques beyond the MF level of approximation. One possibility to face the problem is to calculate higher-order corrections to the 0th-order MF approximation. Tsonchev et al. developed a MF strategy, including leading-order (one-loop) fluctuation corrections, to gain new insights into the physics of confined PE solutions [177]. However, in situations where the MF approximation is bad many computationally demanding higher-order corrections to the integral are necessary, to get the desired accuracy. Another possibility is to make use of MC algorithms and to sample the full partition function integral in field-theoretic representation. However, in a recent work we demonstrated that MC sampling in conjunction with the original field-theoretic representation is impracticable due to the so-called *numerical sign problem* [178]. The difficulty is related to the complex and oscillatory nature of the resulting distribution function, which causes a bad statistical convergence of the functional integral averages of the desired thermodynamic and structural quantities. In such cases special analytical and numerical techniques are necessary to accelerate their statistical convergence [29,178–180]. To make the methodology amenable for computation, we proposed to shift the contour of integration of the partition function integral through the homogeneous MF solution using Cauchy's integral theorem, which was previously successfully employed by Baer et al. in field-theoretic electronic structure calculations [85]. We could demonstrate that this technique provides a significant acceleration of the statistical convergence of the functional integral averages in the MC sampling procedure [178]. Other promising beyond MF simulation techniques have been developed recently, but they either still lack the proof of correct statistical convergence [181,182] and/or still need to prove their effectiveness on systems, where multiple MF solutions are important [180]. In case of the complex Langevin (CL) method [183,184], it is well-known from the field of lattice gauge theory that, due to the introduction of the complex field variable, the general convergence proof is difficult and it is still lacking for general models [44]. Some convergence proofs have been presented, but they are only valid for the specific models and conditions under consideration [185–188]. A rigorous general convergence proof, like in case of MC, would be particularly crucial for slowly converging sampling trajectories occurring in typical beyond MF applications, because in such cases it is very expensive to check the converged results a posteriori against alternative simulation or experimental results. Moreover, the CL method is known to be plagued in many important cases by strong numerical instabilities or subtle ergodic behavior [189]. For these reasons, it has never established itself as a standard simulation algorithm and has essentially been abandoned in the field of lattice gauge theory [190].

4.2.2 Renormalization concepts

An alternative theoretical tool to cope with strong fluctuation problems, arising in SFTs, has been provided in the late 1940s by the concept of renormalization, which has originally been devised to calculate functional integrals occurring in QFT [94,191]. In the latter field one normally makes use of a perturbation theory, to expand the functional integrals in a power series with respect to the coupling parameters. Unfortunately, generally most of the expansion terms turn out to be infinite, thereby rendering such calculations impracticable [191]. A way to remove the infinities from QFT is to make use of the concept of renormalization [192]. It mainly consists in replacing the bare values of the coupling parameters, like e.g. electric charges or masses, by renormalized parameters and requiring that the physical quantities do not change under such a transformation, which leads to finite terms in the perturbation expansion. A simple physical picture of the procedure of renormalization can be drawn from the example of a classical electrical charge Q, which is inserted into a polarizable medium composed e.g. of simple electrolytes. At a distance r from the charge, due to the polarization of the medium, its Coulomb field will effectively depend on a function $Q(r)$, i.e. the effective (renormalized) charge, instead of the bare electrical charge, Q [191]. At the beginning of the 1970s, Wilson further pioneered the power of renormalization concepts by developing the formalism of renormalization group (RG) theory, to investigate critical phenomena of statistical systems [193]. The RG theory makes use of a series of RG transformations, each of which consists of a coarse–graining step followed by a change of scale [34,92,194]. In case of statistical-mechanical problems the steps are implemented by successively eliminating and rescaling the degrees of freedom in the partition sum or integral that defines the model under consideration. The main objective of a RG calculation is to study how parameters in the action and, thus, the form and strength of the interactions among the fluctuating modes are modified by the application of a RG transformation. De Gennes used this strategy to establish an analogy between the behavior of the zero-component classical vector model of ferromagnetism near the phase transition and the self-avoiding random walk of a polymer chain of infinite length on a lattice, which enabled him to calculate the polymer excluded volume exponents [168]. Both Wilson's and de Gennes's seminal contributions in the field of critical phenomena and complex matter were awarded by the Nobel prizes in physics of 1982 and 1991, respectively. Adapting this concept to field-theoretic functional integrals, implies to study in a systematic way, how a SFT model changes while eliminating and rescaling a certain number of degrees of freedom from the partition function integral [34,194]. An alternative approach is known as the *Hartree approximation* or *self-consistent one-loop approximation* [93,195]. It traditionally takes advantage of Gaussian fluctuation corrections to the 0th-order MF contribution, to renormalize the model parameters and extract in a self-consistent way the dominant length scale of the concentration fluctuations in critical concentration regimes [34]. In a more recent work Efimov and Nogovitsin showed that an alternative renormalization technique originating from QFT, based on the concept of *tadpole renormalization*, can be a very effective approach for computing functional integrals arising in statistical mechanics of classical many-particle systems [196,197]. They demonstrated that the main contributions to classical partition function integrals are

provided by low-order tadpole-type Feynman diagrams, which account for divergent contributions due to particle self-interactions. The renormalization procedure performed in this approach effects on the self-interaction contribution of a charge (like e.g. an electron or an ion), which results from the static polarization induced in the vacuum due to the presence of that charge [198]. As evidenced by Efimov and Ganbold in an earlier work [199,200], the procedure of tadpole renormalization can effectively be employed to remove the corresponding divergences from the action of the original field-theoretic representation of the partition function and leads to an alternative functional integral representation, called the *Gaussian equivalent representation* (GER). They showed on the example of the polaron problem that the procedure provides functional integrals with significantly ameliorated approximation characteristics for analytical perturbation calculations [199]. In subsequent works we applied the concept of tadpole renormalization in conjunction with advanced MC techniques in the grand canonical ensemble, and demonstrated that this approach efficiently accelerates the statistical convergence of the desired ensemble averages of simple classical many-particle systems [29,36,37,178,179]. In the following we present effective low-cost approximation methods, based on the tadpole renormalization procedure, and show that they deliver useful results for various polymer and PE solution models. For a better understanding of this renormalization procedure, we derive in the subsequent section the GER for a system of flexible polymer chains, using the method of Efimov and Ganbold [199,200].

4.2.3 Gaussian equivalent representation and its 0th-order approximation

To derive the GER of the grand canonical partition function, let us consider the partition function integral in Eq. 19 and perform the following shift of the integration contour by invoking Cauchy's integral theorem [36]

$$w(\mathbf{r}) \longrightarrow w(\mathbf{r}) + i\psi^{GER}(\mathbf{r}), \tag{35}$$

where $\psi^{GER}(\mathbf{r})$ represents the shifting function of the partition function integral. We then get

$$\begin{aligned}\Xi(\xi, V, \beta) = \gamma_{\bar{\Phi}} \exp\left[\frac{1}{2\beta V^2}\int d\mathbf{r}d\mathbf{r}'\psi^{GER}(\mathbf{r})\bar{\Phi}^{-1}(\mathbf{r}-\mathbf{r}')\psi^{GER}(\mathbf{r}')\right] \\ \times \int \mathcal{D}w \exp\left[-\frac{1}{2\beta V^2}\int d\mathbf{r}d\mathbf{r}' w(\mathbf{r})\bar{\Phi}^{-1}(\mathbf{r}-\mathbf{r}')w(\mathbf{r}')\right. \\ \left. -\frac{i}{\beta V^2}\int d\mathbf{r}d\mathbf{r}'\psi^{GER}(\mathbf{r})\bar{\Phi}^{-1}(\mathbf{r}-\mathbf{r}')w(\mathbf{r}') + \xi Q[i(w+i\psi^{GER})]\right],\end{aligned} \tag{36}$$

where $Q[i(w + i\psi^{GER})]$ is defined via Eq. 17. To derive the GER, we employ the procedure of Efimov and Ganbold [199] and introduce the Gaussian measure $\mathcal{D}\mu_{\bar{\Phi}}[w]$

related to the potential of mean force $\bar{\Phi}$,

$$\mathcal{D}\mu_{\bar{\Phi}}[w] = \gamma_{\bar{\Phi}}\mathcal{D}w \exp\left[-\frac{1}{2\beta V^2}\int d\mathbf{r}d\mathbf{r}' w(\mathbf{r})\bar{\Phi}^{-1}(\mathbf{r}-\mathbf{r}')w(\mathbf{r}')\right], \tag{37}$$

as well as the normal product with regard to this measure via the relations

$$:\exp\left[-iN\int_0^1 ds\ w(\mathbf{R}(s))\right]:_{\bar{\Phi}} = \exp\left[-iN\int_0^1 ds\ w(\mathbf{R}(s))\right]\exp\left(\frac{1}{2}\beta N\bar{\Phi}(0)\right),$$

$$w(\mathbf{R}(s))w(\mathbf{R}'(s')) = :w(\mathbf{R}(s))w(\mathbf{R}'(s')):_{\bar{\Phi}} + \beta\bar{\Phi}(\mathbf{R}(s)-\mathbf{R}'(s')). \tag{38}$$

This implies that

$$\int \mathcal{D}\mu_{\bar{\Phi}}[w]:\exp\left[-iN\int_0^1 ds\ w(\mathbf{R}(s))\right]:_{\bar{\Phi}} = 1. \tag{39}$$

Inserting Eqs. 37 and 38 into Eq. 36, we obtain

$$\begin{aligned}\Xi(\xi,V,\beta) = \exp&\left[\frac{1}{2\beta V^2}\int d\mathbf{r}d\mathbf{r}'\psi^{GER}(\mathbf{r})\bar{\Phi}^{-1}(\mathbf{r}-\mathbf{r}')\psi^{GER}(\mathbf{r}')\right]\\ &\times\int\mathcal{D}\mu_{\bar{\Phi}}[w]\ \exp\left[-\frac{i}{\beta V^2}\int d\mathbf{r}d\mathbf{r}'\psi^{GER}(\mathbf{r})\bar{\Phi}^{-1}(\mathbf{r}-\mathbf{r}')w(\mathbf{r}')\right.\\ &\left.+z\mathcal{Q}[i(w+i\psi^{GER})]\right],\end{aligned} \tag{40}$$

where

$$\begin{aligned}&\mathcal{Q}[i(w+i\psi^{GER})]\\ &=\frac{\int\mathcal{D}\mathbf{R}\exp\left[-\beta U_0[\mathbf{R}]+N\int_0^1 ds\ \psi^{GER}(\mathbf{R}(s))\right]:\exp\left[-iN\int_0^1 ds\ w(\mathbf{R}(s))\right]:_{\bar{\Phi}}}{\int\mathcal{D}\mathbf{R}\exp\left[-\beta U_0[\mathbf{R}]\right]}\end{aligned} \tag{41}$$

and the polymer activity $z = \xi\exp\left(-\beta/2N\bar{\Phi}(0)\right)$. The basic idea of the method of Efimov and Ganbold [199] is to concentrate the main contribution to the partition function integral in a Gaussian measure related to a modified potential $D(\mathbf{r})$ by employing the concept of tadpole renormalization [199]. By considering Eq. 37, the new Gaussian measure can be formulated as

$$\mathcal{D}\mu_D[\sigma] = \gamma_D\ \mathcal{D}w\exp\left[-\frac{1}{2\beta V^2}\int d\mathbf{r}d\mathbf{r}' w(\mathbf{r})D^{-1}(\mathbf{r}-\mathbf{r}')w(\mathbf{r}')\right], \tag{42}$$

where the normalization constant γ_D is defined as in Eq. 21, but replacing the interaction potential $\bar{\Phi}$ with D. Moreover, the normal product according to this measure is defined similarly as in Eq. 38, which implies that

$$: \exp\left[-iN\int_0^1 ds\ w(\mathbf{R}(s))\right] :_D = A^{-1} : \exp\left[-iN\int_0^1 ds\ w(\mathbf{R}(s))\right] :_{\bar{\Phi}} \quad (43)$$

with $A = \exp\left(\frac{1}{2}\beta N(\bar{\Phi}(0) - D(0))\right)$. Introducing Eqs. 42 and 43 into Eq. 40, we obtain for the grand canonical partition function

$$\Xi(\xi, V, \beta) = \frac{\gamma_{\bar{\Phi}}}{\gamma_D} \exp\left[\frac{1}{2\beta V^2}\int d\mathbf{r}d\mathbf{r}'\psi^{GER}(\mathbf{r})\bar{\Phi}^{-1}(\mathbf{r}-\mathbf{r}')\psi^{GER}(\mathbf{r}')\right] \times \int \mathcal{D}\mu_D[w]\ \exp[W_{int}], \quad (44)$$

with

$$W_{int} = -\frac{1}{2\beta V^2}\int d\mathbf{r}d\mathbf{r}' w(\mathbf{r})\left(\bar{\Phi}^{-1}(\mathbf{r}-\mathbf{r}') - D^{-1}(\mathbf{r}-\mathbf{r}')\right) w(\mathbf{r}') - \frac{i}{\beta V^2}\int d\mathbf{r}d\mathbf{r}'\psi^{GER}(\mathbf{r})\bar{\Phi}^{-1}(\mathbf{r}-\mathbf{r}')w(\mathbf{r}') + zA\mathcal{Q}[i(w+i\psi^{GER})] \quad (45)$$

and

$$\mathcal{Q}[i(w+i\psi^{GER})] = \frac{\int \mathcal{D}\mathbf{R}\exp\left[-\beta U_0[\mathbf{R}] + N\int_0^1 ds\ \psi^{GER}(\mathbf{R}(s))\right] : \exp\left[-iN\int_0^1 ds\ w(\mathbf{R}(s))\right] :_D}{\int \mathcal{D}\mathbf{R}\exp[-\beta U_0[\mathbf{R}]]}, \quad (46)$$

while

$$\frac{\gamma_D}{\gamma_{\bar{\Phi}}} = \prod_{\mathbf{G}}\left(\frac{\bar{\Phi}(\mathbf{G})}{D(\mathbf{G})}\right)^{1/2}. \quad (47)$$

Afterwards, we expand in Eq. 46 the exponential term within the double dots in a Taylor series up to second order and take into account the properties of the normal product given in Eq. 38. We then obtain for the exponential term

$$: \exp\left[-iN\int_0^1 ds\ w(\mathbf{R}(s))\right] :_D = 1 - iN\int_0^1 w(\mathbf{R}(s))ds - \frac{N^2}{2}\int_0^1\int_0^1 : w(\mathbf{R}(s))w(\mathbf{R}(s')) :_D\ dsds' + : \exp_2\left[-iN\int_0^1 ds\ w(\mathbf{R}(s))\right] :_D, \quad (48)$$

where the latter contribution contains all expansion terms beyond second order. Inserting the previous expression into Eq. 46 and making use of the second relation of Eq. 38, we can rewrite Eq. 45 as

$$
\begin{aligned}
&W_{int} \\
&= zA \frac{\int \mathcal{D}\mathbf{R} \exp\left[-\beta U_0[\mathbf{R}] + N \int_0^1 ds\ \psi^{GER}(\mathbf{R}(s))\right] : \exp_2\left[-iN \int_0^1 ds\ w(\mathbf{R}(s))\right] :_D}{\int \mathcal{D}\mathbf{R} \exp\left[-\beta U_0[\mathbf{R}]\right]} \\
&\quad + \left\{ zA \frac{\int \mathcal{D}\mathbf{R} \exp\left[-\beta U_0[\mathbf{R}] + N \int_0^1 ds\ \psi^{GER}(\mathbf{R}(s))\right]}{\int \mathcal{D}\mathbf{R} \exp\left[-\beta U_0[\mathbf{R}]\right]} \right. \\
&\qquad \left. - \frac{1}{2V^2} \int d\mathbf{r} d\mathbf{r}' \left(\bar{\Phi}^{-1}(\mathbf{r} - \mathbf{r}') - D^{-1}(\mathbf{r} - \mathbf{r}') \right) D(\mathbf{r} - \mathbf{r}') \right\} \\
&\quad - \left\{ zAiN \frac{\int \mathcal{D}\mathbf{R} \exp\left[-\beta U_0[\mathbf{R}] + N \int_0^1 ds\ \psi^{GER}(\mathbf{R}(s))\right] \int_0^1 w(\mathbf{R}(s)) ds}{\int \mathcal{D}\mathbf{R} \exp\left[-\beta U_0[\mathbf{R}]\right]} \right. \\
&\qquad \left. + \frac{i}{\beta V^2} \int d\mathbf{r} d\mathbf{r}' \psi^{GER}(\mathbf{r}) \bar{\Phi}^{-1}(\mathbf{r} - \mathbf{r}') w(\mathbf{r}') \right\} \\
&\quad - : \left\{ zA \frac{N^2}{2} \frac{\int \mathcal{D}\mathbf{R} \exp\left[-\beta U_0[\mathbf{R}] + N \int_0^1 ds\ \psi^{GER}(\mathbf{R}(s))\right] \int_0^1 \int_0^1 w(\mathbf{R}(s)) w(\mathbf{R}(s'))\, ds ds'}{\int \mathcal{D}\mathbf{R} \exp\left[-\beta U_0[\mathbf{R}]\right]} \right. \\
&\qquad \left. + \frac{1}{2\beta V^2} \int d\mathbf{r} d\mathbf{r}' w(\mathbf{r}) \left(\bar{\Phi}^{-1}(\mathbf{r} - \mathbf{r}') - D^{-1}(\mathbf{r} - \mathbf{r}') \right) w(\mathbf{r}') \right\} :_D . \qquad (49)
\end{aligned}
$$

In order to concentrate the main contribution to the partition function integral in the Gaussian measure $\mathcal{D}\mu_D[w]$, we demand that the linear and quadratic terms in the field $w(\mathbf{r})$ in Eq. 49 vanish. These requirements lead to the so-called GER equations in the following form:

$$
\begin{aligned}
&zAN \frac{\int \mathcal{D}\mathbf{R} \exp\left[-\beta U_0[\mathbf{R}] + N \int_0^1 ds\ \psi^{GER}(\mathbf{R}(s))\right] \int_0^1 w(\mathbf{R}(s)) ds}{\int \mathcal{D}\mathbf{R} \exp\left[-\beta U_0[\mathbf{R}]\right]} \\
&\quad + \frac{1}{\beta V^2} \int d\mathbf{r} d\mathbf{r}' \psi^{GER}(\mathbf{r}) \bar{\Phi}^{-1}(\mathbf{r} - \mathbf{r}') w(\mathbf{r}') = 0, \\
&zAN^2 \frac{\int \mathcal{D}\mathbf{R} \exp\left[-\beta U_0[\mathbf{R}] + N \int_0^1 ds\ \psi^{GER}(\mathbf{R}(s))\right] \int_0^1 \int_0^1 w(\mathbf{R}(s)) w(\mathbf{R}(s'))\, ds ds'}{\int \mathcal{D}\mathbf{R} \exp\left[-\beta U_0[\mathbf{R}]\right]} \\
&\quad + \frac{1}{\beta V^2} \int d\mathbf{r} d\mathbf{r}' w(\mathbf{r}) \left(\bar{\Phi}^{-1}(\mathbf{r} - \mathbf{r}') - D^{-1}(\mathbf{r} - \mathbf{r}') \right) w(\mathbf{r}') = 0, \qquad (50)
\end{aligned}
$$

which can easily be reformulated as

$$
\begin{aligned}
&\psi^{GER}(\mathbf{r}) = -zAN\beta \\
&\quad \times \frac{\int \mathcal{D}\mathbf{R} \exp\left[-\beta U_0[\mathbf{R}] + N \int_0^1 ds\ \psi^{GER}(\mathbf{R}(s))\right] \int_0^1 \bar{\Phi}(\mathbf{R}(s) - \mathbf{r}) ds}{\int \mathcal{D}\mathbf{R} \exp\left[-\beta U_0[\mathbf{R}]\right]},
\end{aligned}
$$

$$D(\mathbf{r}-\mathbf{r}') = \bar{\Phi}(\mathbf{r}-\mathbf{r}') - zAN^2\beta \times \frac{\int \mathcal{D}\mathbf{R} \exp\left[-\beta U_0[\mathbf{R}] + N\int_0^1 ds\ \psi^{GER}(\mathbf{R}(s))\right] \int_0^1\int_0^1 D(\mathbf{R}(s)-\mathbf{r})\bar{\Phi}(\mathbf{r}'-\mathbf{R}(s'))\, dsds'}{\int \mathcal{D}\mathbf{R} \exp\left[-\beta U_0[\mathbf{R}]\right]}. \tag{51}$$

In Fourier representation the previous equations give

$$\begin{aligned}\psi^{GER}(\mathbf{G}) &= -zAN\beta\bar{\Phi}(\mathbf{G}) \times \frac{\int \mathcal{D}\mathbf{R} \exp\left[-\beta U_0[\mathbf{R}] + N\int_0^1 ds\ \psi^{GER}(\mathbf{R}(s))\right] \int_0^1 \exp\left[i\mathbf{G}\mathbf{R}(s)\right] ds}{\int \mathcal{D}\mathbf{R} \exp\left[-\beta U_0[\mathbf{R}]\right]},\\ D(\mathbf{G}) &= \bar{\Phi}(\mathbf{G}) - zAN^2\beta\bar{\Phi}(-\mathbf{G})D(\mathbf{G}) \times \frac{\int \mathcal{D}\mathbf{R} \exp\left[-\beta U_0[\mathbf{R}] + N\int_0^1 ds\ \psi^{GER}(\mathbf{R}(s))\right] \int_0^1\int_0^1 \exp\left[i\mathbf{G}\left(\mathbf{R}(s)-\mathbf{R}(s')\right)\right] dsds'}{\int \mathcal{D}\mathbf{R} \exp\left[-\beta U_0[\mathbf{R}]\right]}.\end{aligned} \tag{52}$$

As a result, we obtain a new exact field-theoretic representation of the grand canonical partition function, namely its Gaussian equivalent representation GER,

$$\Xi(\xi, V, \beta) = e^{-\beta\Omega^0_{GER}} \int \mathcal{D}\mu_D[w] \times \exp\left[zA \frac{\int \mathcal{D}\mathbf{R} \exp\left[-\beta U_0[\mathbf{R}] + N\int_0^1 ds\ \psi^{GER}(\mathbf{R}(s))\right] :\exp_2\left[-iN\int_0^1 ds\ w(\mathbf{R}(s))\right]:_D}{\int \mathcal{D}\mathbf{R} \exp\left[-\beta U_0[\mathbf{R}]\right]}\right], \tag{53}$$

with the 0th-order GER approximation (GER0) of the grand canonical free energy

$$\begin{aligned}\Omega^0_{GER} = \frac{1}{\beta}\ln\frac{\gamma_D}{\gamma_{\bar{\Phi}}} &- \frac{1}{2\beta^2V^2}\int d\mathbf{r}d\mathbf{r}'\psi^{GER}(\mathbf{r})\bar{\Phi}^{-1}(\mathbf{r}-\mathbf{r}')\psi^{GER}(\mathbf{r}')\\ &+\frac{1}{2\beta V^2}\int d\mathbf{r}d\mathbf{r}'\left(\bar{\Phi}^{-1}(\mathbf{r}-\mathbf{r}') - D^{-1}(\mathbf{r}-\mathbf{r}')\right)D(\mathbf{r}-\mathbf{r}')\\ &-\frac{zA}{\beta}\frac{\int \mathcal{D}\mathbf{R} \exp\left[-\beta U_0[\mathbf{R}] + N\int_0^1 ds\ \psi^{GER}(\mathbf{R}(s))\right]}{\int \mathcal{D}\mathbf{R} \exp\left[-\beta U_0[\mathbf{R}]\right]},\end{aligned} \tag{54}$$

where the ratio $\gamma_D/\gamma_{\bar{\Phi}}$ is given by Eq. 47. It is worth noting at this stage that the GER provides an optimized representation of the partition function integral by increasing the influence of the quadratic term in the action with respect to the oscillatory interaction functional. As a consequence, the GER possesses better approximation characteristics [89,201,202] and statistical convergence properties [36,178], than the original field-theoretic representation defined in Eq. 19. In the following we further assume that the shifting function is homogeneous and translation invariant, i.e.

$$\psi^{GER}(\mathbf{r}) = \psi^{GER}(\mathbf{G}=0) = const., \qquad D(\mathbf{r},\mathbf{r}') = D(\mathbf{r}-\mathbf{r}'). \tag{55}$$

Inserting Eq. 55 into Eq. 52, we can rewrite the GER equations as

$$\psi^{GER}(\mathbf{G}=0) = -\beta N\bar{\Phi}(\mathbf{G}=0)\xi\exp\left[-\beta/2ND(0)\right]\exp\left[N\psi^{GER}(\mathbf{G}=0)\right],$$
$$D(\mathbf{G}) = \bar{\Phi}(\mathbf{G}) - zAN^2\beta\bar{\Phi}(-\mathbf{G})D(\mathbf{G})\exp\left[N\psi^{GER}(\mathbf{G}=0)\right] \times\frac{\int\mathcal{D}\mathbf{R}\exp\left[-\beta U_0[\mathbf{R}]\right]\int_0^1\int_0^1\exp\left[i\mathbf{G}\left(\mathbf{R}(s)-\mathbf{R}(s')\right)\right]dsds'}{\int\mathcal{D}\mathbf{R}\exp\left[-\beta U_0[\mathbf{R}]\right]}, \quad (56)$$

with $D(0)=\sum_{\mathbf{G}}D(\mathbf{G})$ and $A=\exp\left(\frac{1}{2}\beta N(\bar{\Phi}(0)-D(0))\right)$. Moreover, by inserting Eq. 55 into Eq. 54, we obtain the GER0 approximation of the grand canonical free energy as

$$\Omega^0_{GER}(\xi,V,\beta,N) = \frac{1}{2\beta}\sum_{\mathbf{G}}\ln\left(\frac{\bar{\Phi}(\mathbf{G})}{D(\mathbf{G})}\right) - \frac{\psi^{GER\,2}(\mathbf{G}=0)}{2\beta^2\bar{\Phi}(\mathbf{G}=0)} + \frac{N\psi^{GER}(\mathbf{G}=0)}{2\beta\bar{\Phi}(\mathbf{G}=0)}D(0) - \frac{\xi}{\beta}\exp\left[N\psi^{GER}(\mathbf{G}=0)\right]\exp\left[-\frac{\beta}{2}ND(0)\right], \quad (57)$$

where the GER potential $D(\mathbf{G})$ and the shifting function $\psi^{GER}(\mathbf{G}=0)$ are given by Eq. 56, while the chemical potential related parameter ξ is provided by Eq. 22.

4.2.4 Concept of effective interactions

Another useful theoretical approach that greatly facilitates the computation of polymer solutions is the concept of *effective interactions* between suitably chosen degrees of freedom in the system under study [37,160,203]. The concept was recently found particularly valuable in the calculation of structure and thermodynamics of a wide variety of soft matter systems [204]. For instance, Louis et al. [203] have shown that it provides accurate structural and thermodynamic information of polymer solutions under good solvent conditions. To this end, they demonstrated that self-avoiding walk polymer chains, immersed in a good solvent, form highly penetrable coils and that the effective pair interactions between their center of mass can well be represented by a repulsive Gaussian potential of the form [205,206]

$$\Phi(r) = \Phi(0)\exp[-(r/R)^2], \quad (58)$$

where $r=|\mathbf{r}|$ is the distance between the interacting coils, while $\Phi(0)$ and R are the energy scale and width of the Gaussian interaction, respectively. In their investigations they demonstrated that this model accurately reproduces the structural and thermodynamic properties of these systems over a large concentration range. In a recent work Konieczky et al. could further show that it also reproduces the characteristic thermodynamic features of solutions of weakly charged PE chains, forming highly penetrable coils as in case of the neutral polymer solutions considered previously, and, thus, constitutes a useful potential model to mimic their effective interactions [160]. By direct comparison of computer simulation results and heat capacity measurements, we have lately shown in our work in Ref. [33] that the Gaussian effective potential also reproduces the characteristic thermodynamic features of micellar aggregates of

ionic surfactants. These findings have recently found additional support through various theoretical and experimental investigations on similar systems [207,208]. In this review we will make use of it, to demonstrate the effectiveness of our low-cost approximation methods introduced previously. Note that in all our calculations, presented in the following, we employed the system of reduced units (r.u.) that is natural for the model [36]. In the subsequent part of this chapter we consider a model of screened Coulomb type, describing the effective interactions between Debye–Hückel (DH) chains [209]. Since the pioneering work of Derjaguin, Landau, Verwey and Overbeek (DLVO) [210–212], it is well-established that the effective interactions between monomers of PE s can well be described by a DH or Yukawa potential of the following form [209]:

$$\Phi(r) = \Phi_0 \left(\frac{a}{r}\right) \exp\left[-\kappa r\right], \tag{59}$$

where a is a typical inter-monomer distance and κ is the DH screening parameter. The latter quantity governs the range of interactions and is a function of the density of the screening ions as well as the dielectric properties of the solution [209]. The prefactor Φ_0 is proportional to the effective charges of the interacting monomers, and in case of the DLVO potential includes the geometrical factor. We performed our investigations on this inter-monomer interaction model, because it allows to easily modify the strength of the effective interactions between the interacting monomers, which, as we demonstrated in our work in Ref. [37], is the primary cause for the fluctuation problem of SFTs. Using both potential models discussed previously, we introduce in Refs. [89,201,202] a new low-cost field-theoretic methodology beyond the MF level of approximation, which can easily be adapted to sophisticated polymer models on various levels of description. To assess its usefulness, we first develop and test it on the computationally less expensive effective-particle model and perform calculations in the range of parameters, where the Gaussian potential suitably describe the effective interactions of neutral polymer or weakly charged PE coils in solution. In Ref. [82] we then present applications of the new methodology to more sophisticated polymer models on the chain-level of description. An outline of these applications will be given in the following.

4.3 Solutions of neutral polymer coils

4.3.1 Grand canonical ensemble

In Ref. [201] we make use of the method of Efimov and Ganbold, to derive the GER of the partition function integral for effective-particle field theories within the grand canonical ensemble, and approximate it to lowest-order, which gives us its 0th-order approximation GER0. Applying our approach to the example of solutions of neutral polymer coils described by the effective polymer coil model given in Eq. 58, we demonstrate that the GER0 approach provides a new low-cost approximation method beyond the MF level, which provides a far more accurate 0th-order approximation of the free energy as well as related thermodynamic and structural quantities, than the MF approach. To show this, we compute important thermodynamic quantities using

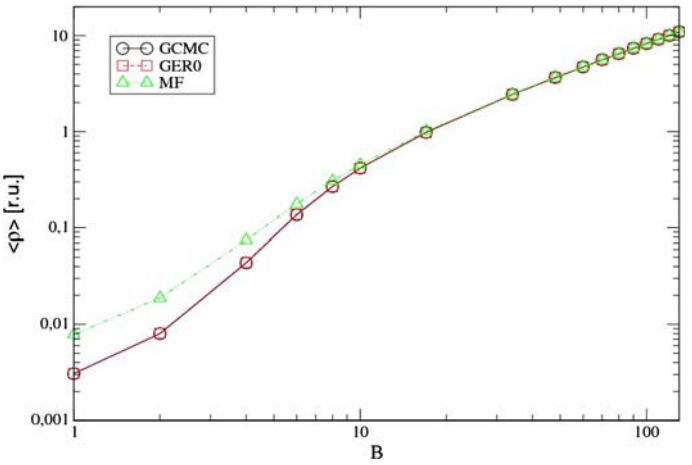

Fig. 14 Average density of polymer coils as a function of the chemical potential-related parameter B. All error bars of the GCMC results are smaller than symbol size

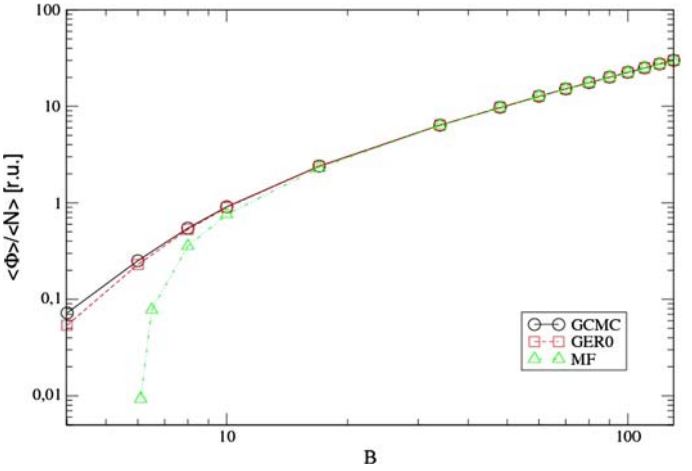

Fig. 15 Average potential energy per average polymer coil number as a function of the chemical potential-related parameter B. All error bars of the GCMC results are smaller than symbol size

our GER0 method and compare the delivered results to non-approximated ones generated with the grand canonical Monte Carlo (GCMC) technique of Norman and Filinov [213]. The GCMC technique relies on the conventional Metropolis MC algorithm [25], to perform the particle displacements. To simulate the particle exchange between the physical system and the particle bath, it incorporates a supplementary particle creation/destruction step into the algorithm. In Figs. 14 and 15 we show the results obtained for the average density of polymer coils and average potential energy per average polymer coil number, calculated with the GER0, MF as well as GCMC method as a function of the chemical potential-related parameter B [201]. We observe that the MF results deviate increasingly with decreasing B-parameter compared to the GCMC results, while the GER0 results remain accurate over the whole parameter range. The discrepancy between the curves, obtained from the GER0 and MF method, grows

dramatically in the low density regime for $\langle \rho^* \rangle < 1.0$. Thus, we conclude from both figures and our work in Ref. [201] that the GER0 approach is an efficient novel low-cost approximation method for grand canonical effective-particle SFTs of neutral polymer solutions beyond the MF level of approximation, which, in contrast to the MF approach, provides accurate results for important thermodynamic quantities over the whole range of polymer coil densities, while requiring similar computational costs.

4.3.2 Canonical ensemble

In our work in Ref. [201] discussed in the previous section, we have introduced the GER0 approach for treating SFTs within the grand canonical ensemble. However, a significant amount of many-body problems of quantum or classical equilibrium statistical mechanics take place at fixed temperature and system size. In our work in Ref. [202] we present a new SCFT for solving canonical ensemble problems over the entire range of coupling parameters, based on the method of GER. We show that the use of the GER procedure in the canonical ensemble case, in contrast to the grand canonical ensemble case, requires the application of a specific transformation procedure to the basic field-theoretic representation of the canonical partition function integral, which is inaccurate at high densities. To cope with the difficulty, we propose in our work in Ref. [202] a *modified GER* procedure, to increase the accuracy of the GER0 approximation in the high density regime. We demonstrate the effectiveness of our canonical ensemble approach on the same model system as discussed in the previous section. In Fig. 16 we present the data obtained for the radial pair distribution function at a reduced polymer coil density of $\rho^* = 0.4$ for various inverse temperatures, using the modified GER0 method. We compare these results to the MF approximation value at $g(r) = 1$ as well as canonical simulation results, generated with the Nosé-Hoover

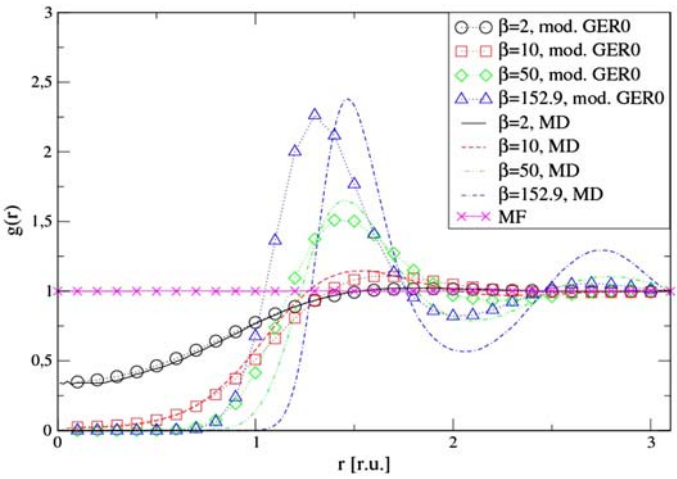

Fig. 16 Radial pair distribution function as a function of the distance of the polymer coils at a density of $\rho^* = 0.4$ for different inverse temperatures, obtained with the modified GER0 approximation, NVT-MD, as well as MF approximation method. All error bars of the NVT-MD results are smaller than symbol size

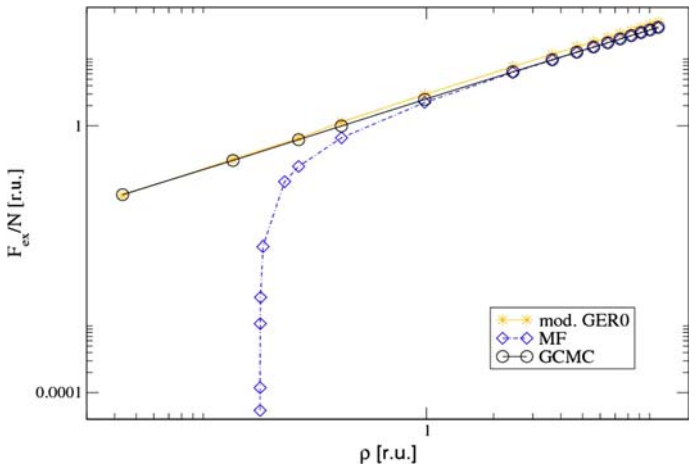

Fig. 17 Excess Helmholtz energy per polymer coil number as a function of the polymer coil density at an inverse temperature of $\beta^* = 2.0$, obtained with the modified GER0 approximation, GCMC, as well as MF approximation method. All error bars of the GCMC results are smaller than symbol size

chain molecular dynamics (NVT-MD) method of Martyna et al. [214]. We see that the modified GER0 results agree qualitatively well with the NVT-MD simulation results in the regime $\beta^* < 50$. Moreover, we notice that the modified GER0 results deviate increasingly from the NVT-MD results with increasing inverse temperature, which is due to the fact that the higher-order corrections to the partition function integral become increasingly important and, thus, need to be taken into account to achieve a higher accuracy in the approximation. These higher-order corrections can e.g. be computed using the modified GER formalism in conjunction with the Metropolis MC algorithm [36,178]. Moreover, we observe that the modified GER0 curve at $\beta^* = 152.9$ is shifted, but reproduce the characteristic features of the non-approximated NVT-MD curve. Finally, it is also worth considering that the curves, provided by the MF approximation, are at $g(r) = 1$ over the whole range of inverse temperatures. This shows that the modified GER0 approximation method introduces a tremendous amount of correlation into the calculation, in contrast to the MF approach, which neither does take into account any correlation nor does provide any information about the structure of the system. Next, in Fig. 17 we show the excess Helmholtz energy per polymer coil number as a function of the polymer coil density at an inverse temperature of $\beta^* = 2$, obtained from the same calculations. We generate the non-approximated comparative free energy data with the GCMC technique of Norman and Filinov [213], since the thermodynamic potential cannot be directly computed with the NVT-MD simulation method. We observe that the modified GER0 results agree well with the ones computed with the GCMC method, while the curve computed with the MF approximation deviates increasingly with decreasing density. In conclusion, we retain from this study that, analogously as in case of the grand canonical ensemble GER0 approach, the canonical GER0 approach is significantly more accurate than the MF approximation over the entire range of polymer coil densities under consideration, while only requiring a negligible amount of additional computational costs. As a consequence,

we conclude that the GER0 approach is also an efficient low-cost approximation technique for calculating SFTs within the canonical ensemble.

4.4 Solutions of weakly charged polymers

Understanding the chemistry and physics of weakly charged polymer systems challenges scientists from a wide spectrum of research areas since many decades [160]. For their efficient numerical treatment, novel SCFT methodologies have emerged recently and proven to provide useful results in case of PE solutions without added salt in the regime of high monomer concentrations [163]. Unfortunately, as we already mentioned in Sect. 2.3, the MF approximation, underlying SCFTs, is known to fail in lower concentration regimes [34], which are of major relevance in most biological and industrial applications. In our work in Ref. [89] we study the suitability of our grand canonical GER0 approach for calculating prototypical open PE systems beyond the MF level of approximation. Since from our work in Ref. [37] we know that the origin of the fluctuation problem in SFTs is related to the strength of the effective interactions between the interacting entities, we test the effectiveness of our method on the example of the effective polymer coil model given in Eq. 58, mimicking in a certain parameter range the effective interactions between weakly charged PE coils [160], and the screened Coulomb model given in Eq. 59, describing the effective inter-monomer interactions of DH chains. We investigate its ability with regard to the MF

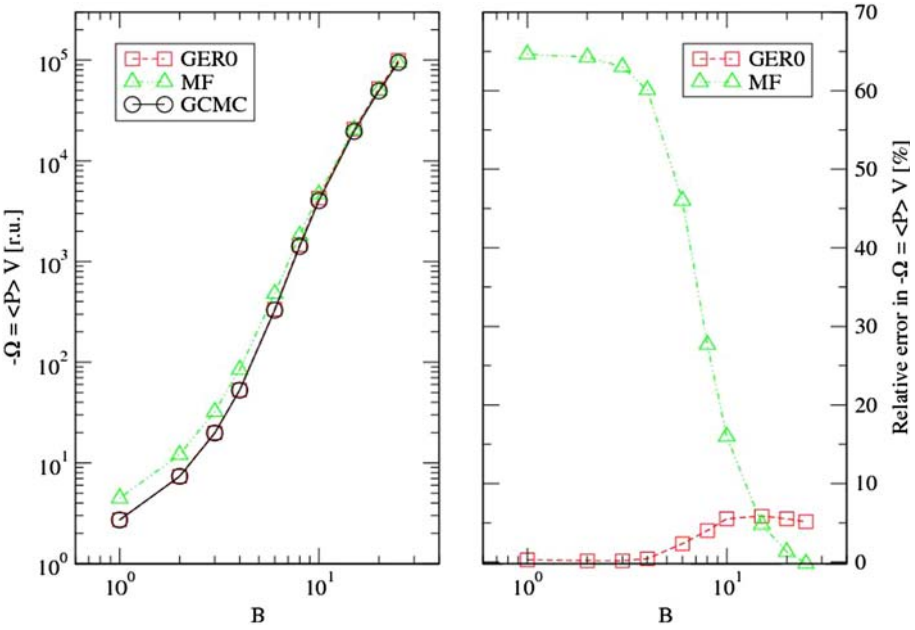

Fig. 18 Grand canonical free energy and corresponding relative error as a function of the chemical potential-related parameter B for the DH inter-monomer interaction model. All error bars of the GCMC results are smaller than symbol size

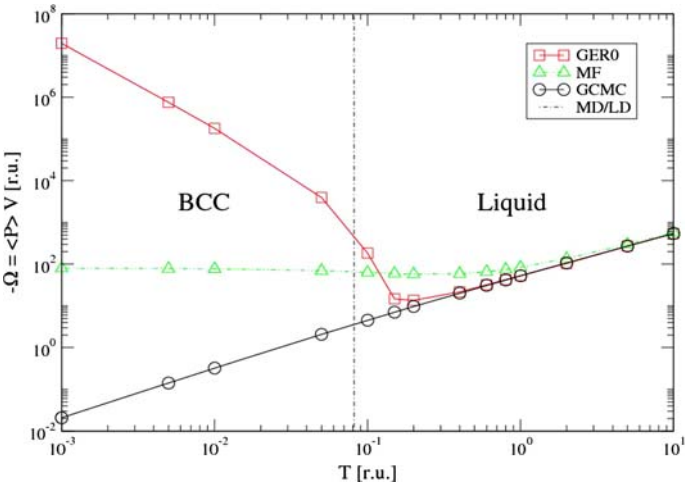

Fig. 19 Grand canonical free energy as a function of the temperature for the DH inter-monomer interaction model. All error bars of the GCMC results are smaller than symbol size

approach, as well as GCMC method of Norman and Filinov [213], in providing accurate thermodynamic information. In Fig. 18 we plot the grand canonical free energy and the corresponding relative error of the DH inter-monomer interaction model as a function of the chemical potential-related parameter B. We observe that the MF results deviate increasingly with decreasing B-parameter with regard to the GCMC results, while the GER0 results coincide well with the GCMC results over the whole B-parameter range. The maximum discrepancy between the relative errors of the MF and GER0 approximation methods in the small B-parameter range amounts to 65%. Furthermore, it is worth pointing out that the GER0 curve of the free energy shows minor deviations in the intermediate B-parameter range with a maximum deviation at $B = 10$. This demonstrates that the accuracy of the GER0 approximation correlates with the strength of the effective interactions, which is the largest in the intermediate B-parameter range [37]. In contrast, we notice that the MF curve does not show this behavior, because the MF approximation does not take into account any correlation at all. Next, in Fig. 19 we visualize the grand canonical free energy for the same model at a fixed B-parameter and volume as a function of temperature, computed with the same methods as in the previous calculations. In addition, we show the location of the liquid-solid phase transition, which only depends on the temperature, determined by Robbins et al. [215] using microcanonical MD and lattice dynamics (LD) calculations. From the figure, we deduce that the curve of the grand canonical free energy, computed with the GER0 method, coincides well with the GCMC simulation data for temperatures $T^* > 0.4$. At smaller temperatures, the GER0 curve deviates increasingly, until it undergoes a severe jump of several orders of magnitude at $T^* \approx 0.15$. We note that the temperature of the jump almost coincides with the temperature of the liquid-BCC phase transition at $T^* \approx 0.08$, determined through the MD and LD calculations previously mentioned. Moreover, we also infer from the graph that at this temperature a discontinuity in the first-order derivative of the grand canonical free energy with respect to

temperature does appear, which is typical for a first-order phase transition. Since the DH model for the range of potential parameters under consideration does not possess a vapor–liquid transition [216], we conclude that the GER0 curve at this temperature reproduces the characteristic features of the liquid-BCC phase transition of the model. In contrast to that, the MF free energy curve shows a minimum and increases slightly with decreasing temperature. Only a small discontinuity in the first-order derivative of the grand canonical free energy with respect to temperature can be deduced from the graph at a temperature of $T^* \approx 0.8$. This value deviates by an order of magnitude from the temperature of the liquid-BCC transition at $T^* \approx 0.08$, obtained from the MD and LD calculations. Furthermore, we note that the curve of the grand canonical free energy, computed with the GCMC approach, does not exhibit any characteristic of the liquid-BCC transition over the entire temperature range. We explain this with the fact that at lower temperatures the kinetic energy of the particles is reduced and, thus, the probability that a cavity is created or destroyed due to fluctuations becomes smaller. Therefore, it becomes more unlikely that a particle can successfully be added to or eliminated from the system, and, as a consequence, the GCMC algorithm fails to provide useful results. Our conclusions concord well with the observations made by Orkoulas and Panagiotopoulos [90], who found in case of ionic systems that grand canonical algorithms become increasingly unreliable with decreasing temperature. To overcome these difficulties, special strategies have been conceived to extend the applicability of the GCMC technique to a wider range of parameters, like e.g. the cavity-biased method of Mezei [217]. New developments essentially based on this approach have recently provided some improved sampling efficiency [218]. However, there is an obvious inherent limitation of the particle-based approaches in their extensibility to the low temperature and/or high density regime, due to their underlying particle exchange algorithm. Other methods make use of extended sampling schemes, in which particles are gradually inserted into the physical system, such as e.g. the grand canonical MD method of Cagin and Pettitt [219–221] or the method of Attard [222]. However, these methods are unphysical in nature, because they do not sample the true grand canonical distribution function. As a consequence, the convergence to the correct thermodynamic averages can never be guaranteed, and these methods have been found to provide wrong results in several important cases [223]. In conclusion, we have demonstrated in our work in Ref. [89] on the example of prototypical PE models that the GER0 approach is a reliable novel low-cost approximation method for calculating SFTs of weakly charged polymer solutions beyond the MF level of approximation. Its computational costs are comparable to the ones of the MF approach, but they are much lower than the costs of the standard GCMC approach. The benefit with respect to the GCMC approach becomes the more crucial the higher the degree of sophistication of the polymer model, i.e. the more molecular details are incorporated into the calculation. Moreover, we have also shown on the example of the screened Coulomb model that the GER0 approach opens new perspectives to reliably determine the phase boundaries of potential models with hard-core repulsion and to extend the range of applicability of the grand canonical ensemble to dense liquid and solid phases of sophisticated PE models.

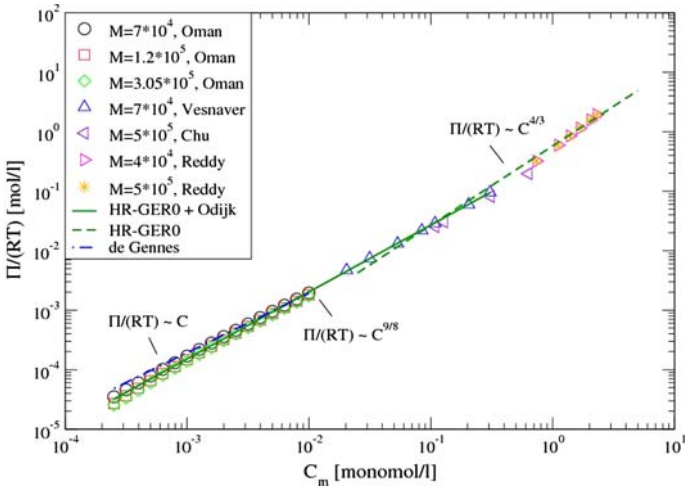

Fig. 20 Osmotic pressure of NaPSS solutions in the dilute and semidilute regime as a function of monomolar concentration without added salt at various molecular weights, obtained with the HR-GER0 approach as well as the Odijk and de Gennes scaling theories in comparison to experimental measurements results. Experimental data are taken from Oman [242], Vesnaver and Skerjanc [243], Chu and Marinsky [244], as well as Reddy and Marinsky [245]

4.5 Solutions of flexible polyelectrolyte chains

In the Sects. 4.3 and 4.4 we discussed the GER0 approach for calculating polymer SFTs beyond the MF level of approximation and presented applications to effective polymer coil models of neutral and weakly charged polymer solutions in high concentration regimes, as well as to the DH inter-monomer interaction model. In our work in Ref. [82] we extend the scope of applicability of the GER approach to PE solutions in moderate to low concentration regimes, where the connectivity of the polymer chains is explicitly taken into account. To this end, we develop a new field-theoretic methodology, which combines the concept of tadpole renormalization of the GER0 approach with the Hartree renormalization procedure and permits to calculate SFTs of solutions composed of flexible neutral or charged polymer chains over the entire range of monomer concentrations. We call this procedure the Hartree renormalized GER0 (HR-GER0) approach and demonstrate its effectiveness on the example of a system of flexible PE chains, where the monomers interact via a DLVO type of pair potential involving excluded volume interactions [33]. With this approach, we analytically derive suitable expressions for the osmotic pressure in all concentration regimes and test their reliability with regard to results obtained from alternative theoretical approaches as well as experimental measurements, performed on sodium poly-(styrene-sulfonate) (NaPSS) PE solutions without and with added salt over the whole range of monomer concentrations. In Fig. 20 we plot the results obtained for the osmotic pressure as a function of monomolar concentration in the dilute and semidilute concentration range, generated with the HR-GER0 approach as well as the scaling theories of Odijk and de Gennes [224–226]. We compare them to experimental data, yielded from NaPSS solutions at various molecular weights. We observe that at low

concentrations the power law with an exponent of 9/8, obtained with the HR-GER0 approach, fits the experimental data very well, while the scaling law of de Gennes with an exponent of 1 deviates increasingly in the low concentration regime from the experimental results with NaPSS of high molecular weight. Moreover, we recognize that with increasing concentration there is an accelerated increase of the osmotic pressure curve and that, at a critical concentration of $\mathcal{C}_m^{ICC} \approx 0.1$ monomol/l, there is a smooth crossover between the power law with exponent 9/8 to a power law with exponent 4/3. We attribute this smooth crossover to the interplay of the phenomena of screening of the monomer charges and self-contraction of the stretched PE chains, leading to a change of the PE shapes. The effect of electrostatic screening of the monomer charges is undertaken by the counterions, which form a diffuse double layer to neutralize the monomer charges of opposite sign [227–229]. The size of this double layer roughly obeys $1/\kappa$, which implies that the size in the semidilute regime is inversely proportional to the square root of the monomer concentration [82]. This dependency of the size of the counterion cloud on concentration can be explained by the fact that only a part of the counterions are condensed onto the sulfonate groups of the NaPSS chains, forming the so-called Stern layer [230]. The rest of the counterions contribute as highly mobile ions to the diffuse double layer surrounding each PE chain and, therefore, they are responsible for the concentration dependence of the screening length κ in the semidilute regime. The size of this double layer is mainly determined by the competition between the thermal motion of the counterions, which tend to spread out or homogenize their distribution in order to increase their entropy, and the electrostatic interactions, which attract the counterions toward the monomer surfaces while repelling the monomers with charges of the same sign [229]. This picture concords well with the findings made by Alexander et al. in case of systems of charged colloids [231]. He discovered that potential models of screened Coulomb type can be applied to a wide range of concentrations, if the bare macroion (monomer) charge is suitably renormalized [231,232]. The physical concept behind this approach relies on the assumption that counterions can tightly bind (condense) onto the fixed surface charges of the macroions and contribute in this way to reduce their bare values, resulting in smaller effective macroion charges. The counterions undergo this condensation process, until the charge densities adjacent to the macroions are reduced below a certain critical threshold [233]. This process is also known as the phenomenon of *counterion condensation* and has led in the late 1960s to the development of the counterion condensation theory for PE solutions by Manning [233]. However, in case of PE solutions this effect goes along with the phenomenon of contraction of the PE chains onto themselves as the concentration of the monomers grows, leading to a rapid increase of the effective monomer charges and interactions. We attribute the change of power law from exponent 9/8 to 4/3 at the critical concentration C_m^{ICC} to a crossover from outer-chain contraction (OCC) to inner-chain contraction (ICC), caused by changing bending properties along the PE chains due to non-uniform counterion condensation. As recently shown by Rubinstein et al. [234] with computer simulations of dilute PE solutions, the center parts of the chains experience strong stretching due to strong Coulomb repulsion of loosely attached counter-ions, which function as a supporting corset. In contrast, the counterions at the outer parts of the chains are attached more tightly, leading to a strong screening of

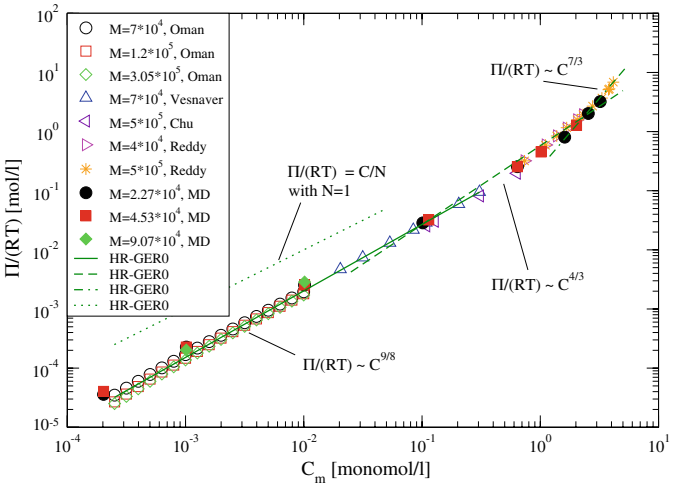

Fig. 21 Osmotic pressure of NaPSS solutions as a function of monomolar concentration over the entire concentration range without added salt and at various molecular weights, obtained with the HR-GER0 approach as well as with the MD method by Stevens and Kremer [232] in comparison to experimental measurements results. Experimental data are taken from Oman [242], Vesnaver and Skerjanc [243], Chu and Marinsky [244], as well as Reddy and Marinsky [245]

the inter-monomer interactions. As a consequence, at the chain ends the tendency of forming a kink is favored over the tendency of elongation due to Coulomb repulsion. This causes that the outer chain segments are somewhat more flexible than the inner chain segments and their probability to contract grows with increasing concentration. Similarly, Stevens and Kremer [235] observed in their MD simulations that, due to counterion condensation, the chains contract significantly before they overlap, forming PEs with horseshoe shape. They argued that the fraction of condensed counterions increases with polymer concentration, leading to a decrease of the effective charges on the chains and causing in this way their contraction. Moreover, they pointed out that the two effects of non-uniform counterion condensation and counterion-mediated chain self-contraction were in the past always ignored in simple scaling theories and, thus, may question their validity. In our HR-GER0 approach these effects are taken into account by renormalizing the monomer charge number in a suitable way. This causes that, besides the length scale associated with the strength of the Coulomb interaction, additional length scales, associated with the both effects previously mentioned, are introduced in our HR-GER0 approach. Next, in Fig. 21 we show the osmotic pressure as a function of the monomolar concentration for solutions of NaPSS PEs at different molecular weights over the whole concentration range, obtained from the HR-GER0 approach as well as experimental measurements, in comparison to the MD simulation results of Stevens and Kremer [232]. The latter authors modeled the PE chains as freely-jointed bead-spring chains, where the charged monomers interacted via the DH pair potential, while the solvent was modeled by a dielectric background. The simulations were performed with chain lengths of $N = 32$ and $N = 64$ beads, as well as at low densities with a chain length of

$N = 128$ beads, while the number of DH chains in the simulation cell was either 8 or 16. Note that we mapped the MD simulation results onto systems of NaPSS PEs in water, making use of the procedure proposed by Stevens and Kremer [232]. We see that, similarly to the MD simulation method, the HR-GER0 approach reproduces the experimental osmotic pressure curves well over the entire concentration range. We recognize that with increasing concentration the experimental data concords increasingly well with the power law with exponent 7/3, obtained using the HR-GER0 approach. A good match is achieved at concentrations starting from $C_m^{OVP} \approx 2$ monomol/l, which represents the critical overlap (OVP) concentration of the crossover from the semidilute to the concentrated regime of the NaPSS PE solutions. In the high concentration range the counterions can be assumed to be almost entirely condensed onto the charged surfaces of the monomers, thereby screening their interactions effectively. As a consequence, in this regime the inter-monomer interactions are short-ranged and the screening length becomes independent of concentration. Due to the effective and almost uniform screening of the counterions, the chains are entirely collapsed onto themselves and form polymer coils, as in case of neutral polymer solutions [34]. This is reflected by a similar scaling exponent of 9/4, derived for the latter case by des Cloizeaux [236,237]. At the critical overlap concentration C_m^{OVP}, the screened PE coils pack to fill the entire space with unit volume fraction and they can be assumed to overlap with each other. By contrast, in the low concentration range, we recognize that the experimental curves, resulting from solutions of NaPSS PEs of different molecular weights, show a considerable scatter. This is a manifestation of the molecular weight dependence of the osmotic pressure in the dilute concentration regime, reflecting the polymeric nature of the PE chains [162]. Moreover, we visualize in the graph the two curves derived for the dilute and semidilute regime, obeying, respectively, a power law with exponent 9/8 and 4/3. We observe that the experimental curves with the NaPSS PEs of intermediate molecular weights of $M = 1.2 \times 10^5$ g/mol and $M = 3.05 \times 10^5$ g/mol obey the theoretically derived power law with exponent 9/8 very well. In contrast, the experimental curve of the low-molecular weight NaPSS PEs with $M = 7 \times 10^4$ g/mol deviates from the power law with exponent 9/8, while being more close to the power law with exponent 1 representing ideal behavior. Thus, we deduce from the graph that the HR-GER0 approach correctly reproduces the molecular weight dependence of NaPSS solutions in the dilute concentration regime and that the ideal behavior is recovered in the limit of short chain lengths. Finally, it is also worth emphasizing that, in contrast to field-theoretic approaches, MD simulations at higher concentrations can only deal with PEs of short chain lengths. This severely limits the scope of application of the MD methodology, since systems of biological and technological interest generally consist of long PE chains, possessing prohibitively long equilibration times [34]. In conclusion, we retain from our study in Ref. [82] that the HR-GER0 approach provides useful osmotic pressure results over the entire range of monomer concentrations by taking advantage of effective renormalization procedures and, in contrast to conventional particle-based simulation methods, also permits to deliver useful results for PE systems with long polymer chains in non-dilute concentration regimes.

5 Quantum systems

Devising theoretical tools for the treatment of structures and dynamical phenomena on the quantum level of description is of particular importance for the development of functionalized polymer materials, like e.g. polymer-based (semi-)conductors [238] or optoelectronic devices [104]. As already outlined in the Sect. 1.1.1, various particle-based quantum-chemical techniques have been developed in recent years, increasing the scope of application of the quantum level significantly. However, their usefulness for polymer systems is generally highly limited, due to their large system sizes and restrictions in computational power [22]. In case of functional-integral-based techniques a lot of efforts have been invested in Feynman's path-integral approach [87]. However, no computationally tractable method for investigating realistic systems could be developed up to now within this methodology. This relates to severe numerical difficulties caused by strong oscillations of the complex integrand at moderate to long propagation times [87]. Very recently, Rom et al. [84,85] introduced a promising novel quantum MC method for performing highly correlated electronic-structure calculations, relying on the field-theoretic formalism. It has successfully been employed to calculate ground-state and low-lying excited states of various atoms and small molecules [86]. However, its application to larger systems has been hindered by a deteriorated statistical convergence [85]. To cope with these difficulties, we have developed in the works introduced subsequently a novel field-theoretic approach for treating quantum-statistical and quantum-dynamical many-body problems, based on the concept of tadpole renormalization. In our publication in Ref. [87] we derive a new field-theoretic representation of the real-time many-body evolution operator, which possesses better approximation characteristics and sampling properties for real-time quantum-dynamical calculations than the original field-theoretic formulation. For this, we make use of a generalized version of the method of Efimov and Ganbold [199], which efficiently eliminates the main divergences from the action caused by the self-interaction contributions of the electrons. In our publication in Ref. [86] we derive a novel field-theoretic representation of the imaginary-time evolution operator, using a similar procedure as in the previous case. The resulting SFT permits to deal with statistical many-body problems on the quantum level of description, as occurring in a multitude of polymer applications. In both cases we demonstrate that in the limit of small timesteps the GER goes over in the so-called MF representation, originally proposed by Rom et al. for electronic-structure calculations [84,85].

6 Conclusions and outlook

In conclusion, we have shown in this review that the field-theoretic formalism is an effective theoretical tool, to solve the multiple length and time scale problems arising in the calculation of the physical properties of a multitude of polymer materials. It possesses the advantageous property that it allows to treat all length scales, spanning from the quantum to the continuum scale, within an unified theoretical framework. As we demonstrated on the example of the coupling of the mesoscopic and continuum scale, this specific feature constitutes a crucial advantage of field-theoretic

approaches versus particle-based simulation methodologies for connecting different levels. Another major benefit relates to their favorable approximation characteristics, which permit to devise efficient coarse–graining strategies for evaluating sophisticated polymer problems in a reliable way. To show this, we have presented novel low-cost approximation strategies beyond the MF level of approximation using effective renormalization concepts, originating from quantum field theories, and demonstrated their usefulness in the calculation of structural and physical properties of several polymer systems, described at various levels of description.

The goal of our future research activity is to adapt and apply the multiscale modeling techniques described in this review, to investigate the structure–property relationship of various inhomogeneous polymer and complex fluid materials, subjected to a nonlinear external perturbation. A particular emphasis will be put on the study of the effect of nanoscale structures and phenomena on the properties of functionalized polymer materials, like the ones occurring in the area of polymer optoelectronics [100], complex foods [239,240] or biomaterials [30]. Such systems characteristically exhibit a hierarchy of different length and time scales, which are correlated with each other and decisively influence the nonlinear material properties. Since they are generally strongly influenced by fluctuations, we will in addition concentrate on further developing efficient low-cost approximation methods beyond the MF level of approximation for calculating the respective statistical field theories in an effective way.

Acknowledgements We wish to thank Glenn H. Fredrickson (UC Santa Barbara, USA), Andrei A. Gusev (ETH Zuerich, Switzerland), Evgenij A. Nogovitsin (Russian Academy of Sciences, Ivanovo, Russia) and Atsushi Hotta (Keio University, Japan) for offering stimulating discussions and for the fruitful collaboration in the field of polymer science. Moreover, we gratefully acknowledge the financial support of this research by Rhodia (France) and Mitsubishi Chemical Corporation (Japan).

References

1. C.J. Hawker, A.W. Bosman, E. Harth, Chem. Rev. **101**, 3661 (2001)
2. W. Kaminsky, P.-D. Tran, U. Weingarten, Macromol. Symp. **193**, 1 (2003)
3. W. Kaminsky, I. Albers, M. Vathauer, Des. Monomers Polym. **5**, 155 (2002)
4. W. Kaminsky, Macromol. Symp. **174**, 269 (2001)
5. J. Baschnagel, K. Binder, P. Doruker, A.A. Gusev, O. Hahn, K. Kremer, W.L. Mattice, F. Müller-Plathe, M. Murat, W. Paul, S. Santos, U.W. Suter, V. Tries, A. Abe, Adv. Polym. Sci. **152**, 41 (2000)
6. D.N. Theodorou, Comput. Phys. Commun. **169**, 82 (2005)
7. A. Ulherr, D.N. Theodorou, Curr. Opin. Solid State Mater. Sci. **3**, 544 (1998)
8. K. Kremer, F. Müller-Plathe, MRS Bull. **26**, 205 (2001)
9. K. Kremer, F. Müller-Plathe, Mol. Simul. **28**, 729 (2002)
10. F. Müller-Plathe, Chem. Phys. Chem. **3**, 754 (2002)
11. F. Müller-Plathe, Soft Mater. **1**, 1 (2003)
12. S.A. Baeurle, A. Hotta, A.A. Gusev, Polymer **46**, 4344 (2005)
13. L.V. Yakushevich, *Nonlinear Physics of DNA* (Wiley-VCH, Weinheim, 2004)
14. R. Das, T.T. Mills, L.W. Kwok, G.S. Maskel, I.S. Millet, S. Doniach, K.D. Finkelstein, D. Herschlag, L. Pollack, Phys. Rev. Lett. **90**, 188103 (2003)
15. S. Tomic, T. Vuletic, S. Dolanski Babic, S. Krca, D. Ivankovic, L. Griparic, R. Podgornik, Phys. Rev. Lett. **97**, 098303 (2006)
16. T. Kottke, B. Dick, R. Fedorov, I. Schlichting, R. Deutzmann, P. Hegemann, Biochemistry **42**, 9854 (2003)
17. S. Crosson, K. Moffat, Proc. Natl. Acad. Sci. **98**, 2995 (2001)
18. M. Praprotnik, K. Kremer, L. Delle Site, Phys. Rev. E **75**, 017701 (2007)

19. J. Rottler, S. Barsky, M.O. Robbins, Phys. Rev. Lett. **89**, 148304 (2002)
20. A. Hotta, S.M. Clarke, E.M. Terentjev, Macromolecules **35**, 271 (2002)
21. G.B. Olson, Science **277**, 1237 (1997)
22. F. Jensen, *Introduction to Computational Chemistry* (Wiley, Chichester, 1999)
23. R.G. Parr, W. Yang, *Density-Functional Theory of Atoms and Molecules* (Oxford University, New York, 1989)
24. P. Hohenberg, W. Kohn, Phys. Rev. **136**, B864 (1964)
25. M.P. Allen, D.J. Tildesley, *Computer Simulation of Liquids* (Clarendon, Oxford, 1996)
26. D. Frenkel, B. Smit, *Understanding Molecular Simulation* (Academic, San Diego, 1996)
27. K. Binder, D.W. Heermann, *Monte Carlo Simulation in Statistical Physics: An Introduction* (Springer, Berlin, 2002)
28. J.M.G. Barthel, H. Krienke, H. Baumgärtel, W. Kunz, *Physical Chemistry of Electrolyte Solutions: Modern Aspects* (Springer, Darmstadt, 1998)
29. S.A. Baeurle, J. Comput. Phys. **184**, 540 (2003)
30. A. Redondo, R. LeSar, Annu. Rev. Mater. Res. **34**, 279 (2004), and references therein
31. T. Aoyagi, T. Honda, M. Doi, J. Chem. Phys. **117**, 8153 (2002)
32. M.J. Stevens, K. Kremer, Phys. Rev. Lett. **71**, 2228 (1993)
33. S.A. Baeurle, J. Kroener, J. Math. Chem. **36**, 409 (2004), and references therein
34. G.H. Fredrickson, *The Equilibrium Theory of Inhomogeneous Polymers* (Clarendon, Oxford, 2006), and references therein
35. K. Kadau, T.C. Germann, P.S. Lomdahl, Int. J. Mod. Phys. C **17**, 1755 (2006)
36. S.A. Baeurle, R. Martonak, M. Parrinello, J. Chem. Phys. **117**, 3027 (2002)
37. S.A. Baeurle, Comput. Phys. Commun. **157**, 201 (2004)
38. M. Doi, S.F. Edwards, *The Theory of Polymer Dynamics* (Oxford University, New York, 1986)
39. R. Faller, Polymer **45**, 3869 (2004)
40. K. Binder, *Monte Carlo and Molecular Dynamics Simulations in Polymer Sciences* (Oxford University, New York, 1995)
41. F. Schmid, J. Phys. Condens. Matter **10**, 8105 (1998)
42. M. W. Matsen, J. Phys. Condens. Matter **14**, R21 (2002)
43. J.-M. Caillol, O. Patsahan, I. Mryglod, Physica A **368**, 326 (2006)
44. G.H. Fredrickson, V. Ganesan, F. Drolet, Macromolecules **35**, 16 (2002)
45. A.F. Terzis, D.N. Theodorou, A. Stroeks, Macromolecules **35**, 508 (2002)
46. A.F. Terzis, D.N. Theodorou, A. Stroeks, Macromolecules **33**, 1385 (2000)
47. A.F. Terzis, D.N. Theodorou, A. Stroeks, Macromolecules **33**, 1397 (2000)
48. P.K. Valavala, G.M. Odegard, Rev. Adv. Mater. Sci. **9**, 34 (2005), and references therein
49. A.A. Gusev, J. Mech. Phys. Solids **45**, 1449 (1997)
50. A.A. Gusev, Macromolecules **34**, 3081 (2001)
51. O.C. Zienkiewicz, R.L. Taylor, *The Finite Element Method, vol. 1: The Basis* (Butterworth-Heinemann, Oxford, 2000)
52. J.W. Eischen, S. Torquato, J. Appl. Phys. **74**, 159 (1993)
53. P.K. Banerjee, *The Boundary Element Methods in Engineering* (McGraw-Hill, London, 1994)
54. S.A. Baeurle, G.H. Fredrickson, A.A. Gusev, Macromolecules **37**, 5784 (2004)
55. M.J. Folkes, A. Keller, Polymer **12**, 222 (1971)
56. M. Takayanagi, H. Harima, Y. Iwata, Mem. Fac. Eng. Kyushu Univ. **23**, 41 (1963)
57. J.M. Whitney, M.B. Riley, Am. Inst. Aeronaut. Astronaut. J. **4**, 1537 (1966)
58. Z. Hashin, J. Mech. Phys. Solids **13**, 119 (1965)
59. R. Hill, J. Mech. Phys. Solids **12**, 199 (1964)
60. Z. Hashin, B.W. Rosen, Trans. ASME **31**, 223 (1964)
61. B.W. Rosen, Proc. Roy. Soc. Lond. Ser. A **319**, 79 (1970)
62. G.A. Van Fo Fy, G.N. Savin, Polym. Mech. **1**, 106 (1965)
63. C.C. Chamis, G.P. Sendeckyj, J. Compos. Mater. **2**, 332 (1968)
64. M. Doi, Macromol. Symp. **195**, 101 (2003)
65. S.C. Glotzer, W. Paul, Annu. Rev. Mater. Res. **32**, 401 (2002)
66. L. Delle Site, C.F. Abrams, A. Alavi, K. Kremer, Phys. Rev. Lett. **89**, 156103 (2002)
67. L. Delle Site, S. Leon, K. Kremer, J. Am. Chem. Soc. **126**, 2944 (2004)
68. L. Delle Site, K. Kremer, Int. J. Quantum Chem. **101**, 733 (2005)
69. M. Neri, C. Anselmi, M. Cascella, A. Maritan, P. Carloni, Phys. Rev. Lett. **95**, 218102 (2005)

70. E. Villa, A. Balaeff, L. Mahadevan, K. Schulten, Multiscale Model. Simul. **2**, 527 (2004)
71. H. Rafii-Tabar, L. Hua, M. Cross, J. Phys.: Condens. Matter **10**, 2375 (1998)
72. J.A. Smirnova, L.V. Zhigilei, B.J. Garrison, Comput. Phys. Commun. **118**, 11 (1999)
73. S.T. O'Connell, P.A. Thompson, Phys. Rev. E **52**, R5792 (1995)
74. N.G. Hadjiconstantinou, Phys. Rev. E **59**, 2475 (1999)
75. J. Li, D. Liao, S. Yip, Phys. Rev. E **57**, 7259 (1998)
76. E.G. Flekkoy, G. Wagner, J. Feder, Europhys. Lett. **52**, 271 (2000)
77. R. Delgado-Buscalioni, P.V. Coveney, Phys. Rev. E **67**, 046704 (2003)
78. J.Q. Broughton, F.F. Abraham, N. Bernstein, E. Kaxiras, Phys. Rev. B **60**, 2391 (1999)
79. A. Laio, J. VandeVondele, U. Röthlisberger, J. Chem. Phys. **116**, 6941 (2002)
80. G. Csanyi, T. Albaret, M.C. Payne, A. De Vita, Phys. Rev. Lett. **93**, 175503 (2004)
81. S.K. Ghosh, Bull. Mater. Sci. **26**, 3 (2003)
82. S.A. Baeurle, E.A. Nogovitsin, Polymer **48**, 4883 (2007)
83. S.F. Edwards, Proc. Phys. Soc. **85**, 613 (1965)
84. N. Rom, D.M. Charutz, D. Neuhauser, Chem. Phys. Lett. **270**, 382 (1997)
85. R. Baer, M. Head-Gordon, D. Neuhauser, J. Chem. Phys. **109**, 6219 (1998)
86. S.A. Baeurle, Int. J. Theor. Phys. **41**, 1915 (2002)
87. S.A. Baeurle, J. Math. Chem. **34**, 29 (2003), and references therein
88. I.S. Aranson, V.A. Kalatsky, V.M. Vinokur, Phys. Rev. Lett. **85**, 118 (2000)
89. S.A. Baeurle, M. Charlot, E.A. Nogovitsin, Phys. Rev. E **75**, 011804 (2007)
90. G. Orkoulas, A.Z. Panagiotopoulos, Fluid Phase Equilib. **83**, 223 (1993), and references therein
91. J.W. Negele, H. Orland, *Quantum Many-Particle Systems* (Perseus Books, Reading, 1998)
92. N. Goldenfeld, *Lectures on Phase Transitions and the Renormalization Group* (Addison-Wesley, New York, 1992)
93. D.J. Amit, *Field Theory, the Renormalization Group and Critical Phenomena* (World Scientific, Singapore, 1984)
94. M. Kaku, *Quantum Field Theory* (Oxford University, New York, 1993)
95. J. Noolandi, T.S. Davison, A.R. Völkel, X.-F. Nie, C. Kay, C.H. Arrowsmith, Proc. Natl. Acad. Sci. **97**, 9955 (2000)
96. E. Helfand, Y. Tagami, J. Polym. Sci. Polym. Lett. **9**, 741 (1971)
97. R.J. Spontak, N.P. Patel, Curr. Opin. Colloid Interface Sci. **5**, 334 (2000)
98. M.J. Folkes, A. Keller, in *Block and Graft Copolymers*, ed. by J.J. Burke, V. Weiss (Syracuse University, Syracuse, 1973), 87 pp
99. A.-V. Ruzette, L. Leibler, Nature Mater. **4**, 19 (2005)
100. A.C. Balazs, T. Emrick, T.P. Russell, Science **314**, 1107 (2006)
101. R.B. Thompson, V.V. Ginzburg, M.W. Matsen, A.C. Balazs, Science **292**, 2469 (2001)
102. J.-Y. Cheng, C.A. Ross, E.L. Thomas, H.I. Smith, G.J. Vancso, Adv. Mater. **15**, 1599 (2001)
103. S. Krishnamoorthy, C. Hinderling, H. Heinzelmann, Mater. Today **9**, 40 (2006)
104. X.-Y. Wang, R.N. Prabhu, R.H. Schmehl, M. Weck, Macromolecules **39**, 3140 (2006)
105. S. Sun, Z. Fan, Y. Wang, J. Haliburton, J. Mater. Sci. **40**, 1429 (2005)
106. S.-S. Sun, Sol. Energy Mater. Sol. Cells **79**, 257 (2003)
107. M.L. Adams, A. Lavasanifar, G.S. Kwon, J. Pharm. Sci. **92**, 1343 (2003)
108. B. Jeong, Y.H. Bae, D.S. Lee, S.W. Kim, Nature **388**, 860 (1997)
109. Y. Kakizawa, K. Kataoka, Adv. Drug Deliv. Rev. **54**, 203 (2002)
110. E. Lavik, R. Langer, Appl. Microbiol. Biotechnol. **65**, 1 (2004)
111. J. Diamant, M.C. Williams, D.S. Soane, Polym. Eng. Sci. **28**, 207 (1988)
112. G. Holden, E.T. Bishop, R. Legge, J. Polym. Sci. Part C **26**, 37 (1969)
113. B. Pukánszky, Eur. Polym. J. **41**, 645 (2005)
114. L.H. Sperling, *Introduction to Physical Polymer Science* (Wiley, New York, 2001)
115. D.J. Read, R.A. Duckett, J. Sweeney, T.C.B. McLeish, J. Phys. D Appl. Phys. **32**, 2087 (1999)
116. A.D. Drozdov, C. Christiansen, Int. J. Eng. Sci. **44**, 205 (2006)
117. R.G.C. Arridge, M.J. Folkes, J. Phys. D: Appl. Phys. **5**, 344 (1972)
118. J.A. Odell, A. Keller, Polym. Eng. Sci. **17**, 8 (1977)
119. P. Allan, R.G.C. Arridge, F. Ehtaiatkar, M.J. Folkes, J. Phys. D Appl. Phys. **24**, 1381 (1991)
120. T.L. Smith, in *Block Polymers*, ed. by S.L. Aggarwal (Plenum, New York, 1970), 137 pp
121. R. Chasset, P. Thirion, in *Proc. Conf. Phys. Non-Cryst. Solids*, ed. by J.A. Prins (North-Holland, Amsterdam, 1965), 345 pp

122. J.G. Curro, P. Pincus, Macromolecules **16**, 559 (1983)
123. J.D. Ferry, *Viscoelastic Properties of Polymers* (Wiley, New York, 1970)
124. J.G. Curro, D.S. Pearson, E. Helfand, Macromolecules **18**, 1157 (1985)
125. G.B. McKenna, R.J. Gaylord, Polymer **29**, 2027 (1988)
126. A.A. Gurtovenko, Y.Y. Gotlib, J. Chem. Phys. **115**, 6785 (2001), and references therein
127. K.L. Ngai, J. Phys. Condens. Matter **12**, 6437 (2000)
128. T. Inoue, M. Moritani, T. Hashimoto, H. Kawai, Macromolecules **4**, 500 (1971)
129. P.L. Drzal, K.R. Shull, Macromolecules **36**, 2000 (2003)
130. L.D. Landau, E.M. Lifshitz, *Statistical Physics Part I, Volume 5 of Course of Theoretical Physics* (Pergamon, Oxford, 1980), 333 pp
131. S.A. Baeurle, T. Usami, A.A. Gusev, Polymer **47**, 8604 (2006)
132. B.J. Dair, A. Avgeropoulos, N. Hadjichristidis, E.L. Thomas, J. Mater. Sci. **35**, 5207 (2000)
133. C.P. Henderson, M.C. Williams, Polymer **26**, 2021 (1985)
134. C.P. Henderson, M.C. Williams, Polymer **26**, 2026 (1985)
135. B. Morèse-Séguéla, M. St-Jacques, J.M. Renaud, J. Prud'homme, Macromolecules **13**, 100 (1980)
136. G. Kraus, K.W. Rollmann, J. Polym. Sci. Polym. Phys. Ed. **14**, 1133 (1976)
137. P.L. Kumler, S.E. Keinath, R.F. Boyer, Polym. Eng. Sci. **17**, 613 (1977)
138. G. Stöppelmann, W. Gronski, A. Blume, Polymer **31**, 1838 (1990)
139. T.A. Huy, L.H. Hai, R. Adhikari, R. Weidisch, G.H. Michler, K. Knoll, Polymer **44**, 1237 (2003)
140. S.A. Baeurle, A. Hotta, A.A. Gusev, Polymer **47**, 6243 (2006)
141. J.H. Gibbs, E.A. Di Marzio, J. Chem. Phys. **28**, 373 (1958)
142. J.H. Gibbs, J. Chem. Phys. **25**, 185 (1956)
143. E.A. Di Marzio, J.H. Gibbs, J. Chem. Phys. **28**, 807 (1958)
144. E.A. Di Marzio, A.J.M. Yang, J. Res. Natl. Inst. Stand. Technol. **102**, 135 (1997)
145. H. Eyring, T. Ree, Proc. Natl. Acad. Sci. **47**, 526 (1961)
146. C.C. Hsu, H. Eyring, Proc. Natl. Acad. Sci. **69**, 1342 (1972)
147. M.T. Cicerone, F.R. Blackburn, M.D. Ediger, Macromolecules **28**, 8224 (1995)
148. S. Merabia, P. Sotta, D. Long, Eur. Phys. J. E **15**, 189 (2004)
149. S.W. Sides, G.H. Fredrickson, Polymer **44**, 5859 (2003)
150. J.F. Beecher, L. Marker, R.D. Bradford, S.L. Aggarwal, J. Polym. Sci. Part C **26**, 117 (1969)
151. R.A. Robinson, E.F.T. White, in *Block Polymers*, ed. by S.L. Aggarwal (Plenum, New York, 1970), 123 pp
152. C.H. Park, J.H. Kim, M. Ree, B.H. Sohn, J.C. Jung, W.C. Zin, Polymer **45**, 4507 (2004)
153. A.A. Griffith, Philos. Trans. R. Soc. London A **221**, 163 (1921)
154. M. Shen, E.H. Cirlin, D.H. Kaelble, J. Polym. Sci. Polym. Lett. Ed. **8**, 149 (1970)
155. D.F. Leary, M.C. Williams, J. Polym. Sci. Polym. Lett. Ed. **8**, 335 (1970)
156. E. Helfand, Z.R. Wassermann, Polym. Eng. Sci. **17**, 582 (1977)
157. J. Diamant, M.C. Williams, Polym. Eng. Sci. **29**, 227 (1989)
158. M. Hara, *Polyelectrolytes: Science and Technology* (Marcel Dekker, New York, 1993)
159. H. Dautzenberg, W. Jaeger, J. Kotz, B. Philipp, Ch. Seidel, D. Stscherbina, *Polyelectrolytes: Formation, Characterization and Application* (Hanser Gardner, Munich, 1994)
160. M. Konieczky, C.N. Likos, H. Löwen, J. Chem. Phys. **121**, 4913 (2004)
161. N. von Solms, Y.C. Chiew, J. Chem. Phys. **118**, 4321 (2003)
162. L. Wang, V.A. Bloomfield, Macromolecules **23**, 804 (1990), and references therein
163. Q. Wang, T. Taniguchi, G.H. Fredrickson, J. Phys. Chem. B **108**, 6733 (2004)
164. V. Vlachy, A.D.J. Haymet, J. Chem. Phys. **84**, 5874 (1986)
165. R. Chang, A. Yethiraj, Macromolecules **38**, 607 (2005)
166. S. Förster, V. Abetz, A.H.E. Müller, Adv. Polym. Sci. **166**, 173 (2004)
167. A.S. Kimerling, W.E. Rochefort, S.R. Bhatia, Ind. Eng. Chem. Res. **45**, 6885 (2006)
168. P.-G. de Gennes, Phys. Lett. **38A**, 339 (1972)
169. M.W. Matsen, J. Phys. Condens. Matter **14**, R21 (2002)
170. E. Reister, M. Müller, K. Binder, Phys. Rev. E **64**, 041804 (2001)
171. M.W. Matsen, G.H. Griffiths, R.A. Wickham, O.N. Vassiliev, J. Chem. Phys. **124**, 024904 (2006)
172. M. Müller, F. Schmid, Adv. Polym. Sci. **185**, 1 (2005)
173. M. Müller, K. Katsov, M. Schick, Phys. Rep. **434**, 113 (2006)
174. K.C. Daoulas, M. Müller, J. Chem. Phys. **125**, 184904 (2006)
175. H. Frusawa, J. Phys. Condens. Matter **17**, L241 (2005)

176. R.R. Netz, D. Andelman, Phys. Rep. **380**, 1 (2003)
177. S. Tsonchev, R.D. Coalson, A. Duncan, Phys. Rev. E **60**, 4257 (1999)
178. S.A. Baeurle, Phys. Rev. Lett. **89**, 080602 (2002)
179. S.A. Baeurle, Comput. Phys. Commun. **154**, 111 (2003)
180. A.G. Moreira, S.A. Baeurle, G.H. Fredrickson, Phys. Rev. Lett. **91**, 150201 (2003)
181. V. Ganesan, G.H. Fredrickson, Europhys. Lett. **55**, 814 (2001)
182. A. Alexander-Katz, A.G. Moreira, G.H. Fredrickson, J. Chem. Phys. **118**, 9030 (2003)
183. J.R. Klauder, J. Phys. A: Math. Gen. **16**, L317 (1983)
184. H. Gausterer, J.R. Klauder, Phys. Lett. B **164**, 127 (1985)
185. S. Lee, Nucl. Phys. B **413**, 827 (1994)
186. H. Gausterer, S. Lee, J. Stat. Phys. **73**, 147 (1993)
187. H. Gausterer, J. Phys. A: Math. Gen. **27**, 1325 (1994)
188. H. Gausterer, H. Thaler, J. Phys. A: Math. Gen. **31**, 2541 (1998)
189. L. Moriconi, M. Moriconi, Phys. Rev. E **72**, 016125 (2005)
190. C. Adami, S.E. Koonin, Phys. Rev. C **63**, 034319 (2001)
191. D.V. Shirkov, CERN Courier **41**, 14 (2001)
192. S. Weinberg, *The Quantum Theory of Fields* (Cambridge University, Cambridge, 1995)
193. K.G. Wilson, Phys. Rev. B **4**, 3184 (1971)
194. K.G. Wilson, J. Kogut, Phys. Rep. C **12**, 75 (1974)
195. P.M. Chaikin, T.C. Lubensky, *Principles of Condensed Matter Physics* (Cambridge University, Cambridge, 1995)
196. G.V. Efimov, E.A. Nogovitsin, Physica A **234**, 506 (1996)
197. G.V. Efimov, E.A. Nogovitsin, Russ. J. Phys. Chem. **76**, 1877 (2002)
198. Y.G. Yi, arXiv:physics/0010080 v13 (2002) 15 Dec
199. G.V. Efimov, G. Ganbold, Phys. Stat. Sol. **168**, 165 (1991)
200. M. Dineykhan, G.V. Efimov, G. Ganbold, S.N. Nedelko, *Oscillator Representation in Quantum Physics* (Springer, Berlin, 1995), 280 pp
201. S.A. Baeurle, G.V. Efimov, E.A. Nogovitsin, Europhys. Lett. **75**, 378 (2006)
202. S.A. Baeurle, G.V. Efimov, E.A. Nogovitsin, J. Chem. Phys. **124**, 224110 (2006)
203. A.A. Louis, P.G. Bolhuis, J.P. Hansen, Phys. Rev. E **62**, 7961 (2000)
204. C.N. Likos, Phys. Rep. **348**, 267 (2001)
205. F.H. Stillinger, T.A. Weber, J. Chem. Phys. **68**, 3837 (1978)
206. F.H. Stillinger, D.K. Stillinger, Physica A **244**, 358 (1997)
207. G. Massiera, L. Ramos, C. Ligoure, E. Pitard, Phys. Rev. E **68**, 021803 (2003)
208. C. Ligoure, J. Phys. Condens. Matter **17**, S2911 (2005)
209. T.B. Liverpool, M. Stapper, Europhys. Lett. **40**, 485 (1997)
210. B.V. Derjaguin, Kolloid Z. **69**, 155 (1934)
211. B.V. Derjaguin, L.D. Landau, Acta Physicochim. URSS **14**, 633 (1941)
212. E.J. Verwey, J.T.G. Overbeek, *Theory of the Stability of Lyophobic Colloids* (Elsevier, Amsterdam, 1948)
213. G.E. Norman, V.S. Filinov, High Temp. (USSR) **7**, 216 (1969)
214. G.J. Martyna, M.E. Tuckerman, D.J. Tobias, M.L. Klein, Mol. Phys. **87**, 1117 (1996)
215. M.O. Robbins, K. Kremer, G.S. Grest, J. Chem. Phys. **88**, 3286 (1988), and references therein
216. M. Dijkstra, R. van Roij, J. Phys. Condens. Matter **10**, 1219 (1998)
217. M. Mezei, Mol. Phys. **40**, 901 (1980)
218. R.M. Shroll, D.E. Smith, J. Chem. Phys. **110**, 8295 (1999), and references therein
219. T. Cagin, B.M. Pettitt, Mol. Simul. **6**, 5 (1991)
220. T. Cagin, B.M. Pettitt, Mol. Phys. **72**, 169 (1991)
221. J. Ji, T. Cagin, B.M. Pettitt, J. Chem. Phys. **96**, 1333 (1992)
222. P. Attard, J. Chem. Phys. **107**, 3230 (1997)
223. S. Weerasinghe, B.M. Pettitt, Mol. Phys. **82**, 897 (1994)
224. T. Odijk, Macromolecules **12**, 688 (1979)
225. P.-G. de Gennes, P. Pincus, R.M. Velasco, F. Brochard, J. Phys. (Paris) **37**, 1461 (1976)
226. P.-G. de Gennes, *Scaling Concepts in Polymer Physics* (Cornell University, Ithaca, 1979)
227. G. Gouy, J. Phys. **9**, 457 (1910)
228. D.L. Chapman, Philos. Mag. **25**, 475 (1913)
229. J.-P. Hansen, H. Löwen, Annu. Rev. Phys. Chem. **51**, 209 (2000)

230. O. Stern, Z. Elektrochem. **30**, 508 (1924)
231. S. Alexander, P.M. Chaikin, P. Grant, P.J. Morales, P. Pincus, D. Hone, J. Chem. Phys. **80**, 5776 (1984)
232. M.J. Stevens, K. Kremer, J. Phys. II France **6**, 1607 (1996)
233. G.S. Manning, J. Chem. Phys. **51**, 924 (1969)
234. Q. Liao, A.V. Dobrynin, M. Rubinstein, Macromolecules **36**, 3386 (2003)
235. M. Stevens, K. Kremer, J. Chem. Phys. **103**, 1669 (1995)
236. J. des Cloizeaux, J. Phys. (Paris) **36**, 281 (1975)
237. J. des Cloizeaux, J. Phys. (Paris) **36**, 1199 (1975)
238. J. Janata, M. Josowicz, Nature Mater. **2**, 19 (2003), and references therein
239. R. Mezzenga, P. Schurtenberger, A. Burbidge, M. Michel, Nature Mater. **4**, 729 (2005)
240. R. Mezzenga, W.B. Lee, G.H. Fredrickson, Trends Food Sci. Technol. **17**, 220 (2006)
241. R. Adhikari, G.H. Michler, T. An Huy, E. Ivan'kova, R. Godehardt, W. Lebek, K. Knoll, Macromol. Chem. Phys. **204**, 488 (2003)
242. S. Oman, Makromol. Chem. **178**, 475 (1977)
243. G. Vesnaver, J. Skerjanc, J. Phys. Chem. **90**, 4673 (1986)
244. P. Chu, J.A. Marinsky, J. Phys. Chem. **71**, 4352 (1967)
245. M. Reddy, J.A. Marinsky, J. Phys. Chem. **74**, 3884 (1970)